Dispersion of upconverting nanostructures of $CePO_4$ using rod and semi-spherical morphologies into transparent PMMA/PU IPNs by the sequential route

D. Palma-Ramírez[*a] M.A. Domínguez-Crespo*[a], A.M. Torres-Huerta[a], V.A. Escobar-Barrios[b], H. Dorantes-Rosales[c] and H. Willcock[d].

[a]Instituto Politécnico Nacional, CICATA-Altamira, km 14.5 Carretera Tampico-Puerto Industrial Altamira. C.P. 89600, Altamira, Tamps., México.

[b]IPICYT, División de Materiales Avanzados, SLP, México.[c]Instituto Politécnico Nacional, ESIQIE, Departamento de Metalurgia, C.P. 07300, Ciudad de México, México.

[d]Department of Materials, Loughborough University, Loughborough LE11 3TU, United Kingdom

*Corresponding authors: mdominguezc@ipn.mx, d.palma.rmz@gmail.com

ABSTRACT

Upconverting luminescent poly(methylmethacrylate)(PMMA)/poly(urethane)(PU) interpenetrating polymer network (IPN) nanohybrids were prepared using a sequential polymerisation incorporating different wt.% of cerium phosphate ($CePO_4$) nanoparticles. The effect of miscibility/compatibility of the different PMMA/PU ratios, the addition and dispersion of rod and semi-spherical nanostructures in as well as the performance of selected IPNs under accelerated aging were studied using morphological, emission, thermal and mechanical studies. Structural studies revealed that there were physical interactions between C=O groups and $CePO_4$ in PMMA/PU IPNs. The addition of a higher wt.% of nanostructures was found to decrease the transparency of the IPNs. Resulting PMMA/PU/$CePO_4$ IPN nanohybrids are photoluminescent under UV-light, supporting the prolongate of lifetime while maintaining the mechanical properties after being subjected to accelerated weathering. The addition of semi-spherical particles resulted in a more stable materials after accelerated weathering than nanorods.

Keywords: Ductile nanorods and semi-spherical nanostructures; Up-converting PMMA/PU/$CePO_4$ IPNs, Optical properties.

1.0 Introduction

The design of materials with a high transmittance in the visible range, minimum heat loss, high structural strength and good durability is a challenge in the research of transparent or translucent structural panel for applications as bendable displays,

airplane canopies/windows, and light transmitting electromagnetic wave shielding material [1].

Transmittances above 80 % in the solar spectrum and a glass transition temperature (T_g) higher than 100 °C to avoid the greenhouse effect are some of the main requirements in this class of materials [2]. Poly (methyl methacrylate) (PMMA) and poly (carbonate) (PC) sheets are the most common polymeric materials used in glazing [3]. However, the toughness, thermal stability and photophysical performance used to protect them against UV radiation depend on a number of both chemical and physical properties, thus it is highly desirable to improve these properties for building applications [4, 5].

A typical method to improve and reinforce the diverse properties of PMMA, whilst maintaining the transparency, is by combining it with other polymer networks such as the flexible poly(urethane) and form interpenetrating polymer networks (IPNs) [6]). IPNs consist of two or more **cross-linked** polymers with no covalent bonds between the phases and have synergistic properties and superior mechanical properties compared to the individual homopolymers [6]. In particular, transparent PMMA/Poly(urethane) IPNs have actually been reported as possible candidates for applications such as bullet-proof glass and ultra-durable self-cleaning surfaces [7, 8]. Research into hybrid IPNs has also grown in recent years as they offers a unique opportunity to prepare enhanced performance materials by combining the properties of the incompatible organic-inorganic phases involved [6, 9]. Among these inorganic phases, Fluoro-functionalized nanostructured silica (F-SiO_2), silica (SiO_2), carbon black (CB), barium titanate ($BaTiO_3$) and polyaniline haven been incorporated into these systems [8, 10-14].

In this context, cerium phosphate ($CePO_4$) has been proposed as a UV absorber to delay the degradation provoked by the structural damage of plastics used in outdoor applications [15, 16]. As a consequence of its reduced dimensionality and well-defined 4f-5d and 4f-4f electronic transitions allowed, $CePO_4$ has huge potential as a promising material for up-conversion emission applications which have not been well studied into interpenetrating polymer networks [17].

In previous work, the morphology of $CePO_4$ nanostructures was found to be dependent on the pH used during their synthesis. Acid and alkaline conditions formed nanorods and semi-spherical morphologies, respectively [15, 16]. Our hypothesis in undertaking this work is that these different morphologies can reinforce mechanically polymers

such as PMMA/PU IPNs by imparting ductility and converting the incident UV light into a less damaging radiation form (visible range) and therefore preventing the bulk of degradation. Nonetheless, it is essential to understand the mechanism by which the semi-spherical or rod morphologies are incorporated into the PMMA/PU IPNs as well to determine the effect of morphology on properties.

To achieve this goal, it is necessary to study the conditions to obtain transparent and non-separated phases between PMMA and PU in IPNs by evaluating the compatibility/miscibility since it is well known that the synthesis is prone to full gelation and requires careful control of the net-to-net entanglement [8].

Therefore, the present study describes the conditions to obtain high performance PMMA/PU/$CePO_4$ IPNs. The addition of a ductile and aliphatic polyurethane into PMMA was varied between 10-50 wt.% to improve the mechanical properties and study its influence on the structural, thermal and morphological properties. In addition, varying amounts of the nanoparticle were added into PMMA/PU IPNs to determine the effect on nanoparticle/polymer interactions, the dispersion, morphology, photophysical features and thermal properties. Results from evaluation by tensile test (Tensile strength, Young modulus and elongation) of aging in heat/humidity conditions (500 h), and data of hardness and data of hardness and elastic modulus of accelerated weathering in UV/humidity (500 h) are reported. Improved in mechanical properties (strength and ductility) and prolongation of lifetime are benefits that flexible PU, nanorods and semi-spherical nanoparticles can provide in transparent PMMA/PU IPNs.

Further, this work reveals that physical interactions between polymers and nanoparticles including the dispersion, govern the final properties of the PMMA/PU/$CePO_4$ IPNs.

2.0 Experimental

2.1 Materials

Methyl methacrylate (MMA, 99%), trimethylolpropane trimethacrylate (TMPTMA), 1-hydroxycyclohexyl phenyl ketone photoinitiator (HPK, ≥ 99%), hexamethylene diisocyanate (HDI, ≥98%), poly (tetrahydrofuran) (PTHF, **average molecular number** ~650), trimethylolpropane (TMTP, ≥ 98.0%) dibutyltin dilaurate (DBTDL,

95%) and tetrahydrofuran (THF, ≥ 99.99%) were purchased from Sigma Aldrich and used as received. MMA, TMPTMA and HDI were stored over molecular sieves.

2.2 PMMA/PU synthesis

IPNs were prepared by mixing TMTP (0.012 **eq.)** and PTHF (0.012 **eq.)** in a vial sealed with a rubber septum cap at 70 °C under nitrogen atmosphere for 1 h. The mixture was allowed to cool to room temperature, thereafter HDI monomer, MMA monomer, TMPTMA cross-linking agent and HPK photoinitiator were added and stirred for 1 h. Then, DBTDL catalyst was added to this mixture and stirred for 10 min. The final solution was poured into a PTFE **mould** and kept for 18 h and 3 h in UV lamp (313 nm). During the synthesis, it was observed a phase separation when 5 to 10 wt.% of PU was added to form PPMA/PU IPNs (See supplementary material in **Figure I**). For this reason, higher ratios of PMMA/PU in 80/20, 70/30, 60/40 and 50/50 wt. % were only presented in this study, using two mixing times (10 and 60 min).

2.3 PMMA/PU/$CePO_4$ hybrid IPNs

$CePO_4$ nanostructures with nanorod and semi-spherical morphologies with monoclinic structure were synthesized at pH 1 and 11, respectively, by the microwave-assisted hydrothermal method following the procedure described in [16].

Different amounts (0.1, 0.5 and 1.0 wt.%) of both nanostructures, TMTP/THF mixture, HDI monomer, MMA monomer, TMPTMA cross-linking agent and HPK photoinitiator were sonicated for 3 h. DBTDL catalyst was added into the solution and sonicated for 10 min (Figure II in supplementary material). The final solution was poured into a PTFE **mould** and kept for 18 h and 3 h in UV lamp (363 nm).

2.4 Samples characterisation

Differential scanning calorimetry (DSC) and thermogravimetric analysis (TGA) were conducted using a simultaneous Labsys Evo, Setaram TGA/DSC. Samples of DSC were tested at a heating rate of 10 K/min over the temperature range from 30 to 250 °C, under nitrogen atmosphere. 10-20 mg of each sample was placed in aluminium crucibles and maintained at 30 °C for 2 min, heated from 30 °C to 250 °C, maintained

again at 250 °C for 2 min, cooled from 250 °C to 50 °C. Then, samples were scanned from 50 °C to 500 °C to evaluate the decrosslinking and degradation.

Morphology of 50/50, 60/40, 70/30 and 80/20 pure PMMA/PU IPNs was analysed by scanning electron microscopy (SEM) using a JEOL JSM-6701F microscope (5 kV of acceleration voltage). Samples were fractured after cooling in liquid nitrogen before being analysed.

Morphology and structure of $CePO_4$ were investigated by electron transmission microscopy (TEM) using a JEM-2000 FX electron microscope (JEOL) equipped with the selected area electron diffraction (SAED) patterns working at an accelerating voltage of 200 kV.

Fluorescence measurements of nanorods and semi-spherical nanoparticles as well as PMMA/PU/$CePO_4$ were developed on a Carl ZEISS microscope confocal (LSM 700). Spectra were acquired at 405 nm at room temperature. The fluorescence intensity measurements were performed using the built-in software ZEN of the LSM 710.

Fourier Transform Infrared spectra of PMMA/PU and PMMA/PU/$CePO_4$ IPNs in film shapes were obtained using a Nicolet iS5 (Thermo scientific) spectrometer fitted with an **iD7 diamond** attenuated total reflectance (ATR) accessory. Samples were scanned 16 times at the maximum resolution (4.0 cm^{-1}) in the 4000-650 cm^{-1}.

Spectra of PMMA/PU/$CePO_4$ IPNs in the visible range were acquired in a Cary 5000 UV/Vis scanning single beam spectrophotometer in the 400-700 nm, collected with a scan rate of 600 nm min^{-1}, data interval of 1 nm, and average time of 0.1 s.

SEM images and energy dispersive X-ray spectroscopy (EDS) elemental analysis and mapping of selected PMMA/PU/$CePO_4$ samples (50/50 and 80/20 wt.%) were obtained on a Field Emission microscope (JSM-7800F) at 20 kV. Samples were sputter coated with Au-Pd for 30 seconds on a Quorum Q150T ES sputter coater system.

Contact angle (C.A.) measurements were acquired on a Contact Angle System OCA. A drop of 2.0 µL of water as probe liquid was deposited on the samples surfaces through a syringe. Images were acquired by a video camera using the Dataphysics software. The reported angles were calculated with the software from the shape of the drop. Results are the average of at least 5 measurements of CA of droplets at different places on the surface of the IPNs.

Samples were casted in PTFE moulds to obtain sheets with thicknesses of 1 mm. Sheets were cut into tensile dog-bone specimens in according the European Standard

EN ISO 527-2. Tensile test was conducted in an Instron universal testing machine (Model 5944) at a crosshead speed of 20 mm/min by using a load cell of 2 kN. Data were recorded in the Instron software with averages of 4 replicates.

Selected dog-bone specimen of PMMA/PU/$CePO_4$ were subjected to ageing under humid conditions using a climate chamber (Memmer GmbH equipment) at 55 °C and 85 % relative humidity for 500 h. The aged dog-bones were tested by tensile test using the conditions mentioned above.

Specimens were subjected to UV radiation in a Fluorescent UV/Condensation weathering instrument under the ASTM G154 at wavelength of 340 nm. This device was equipped with UV-340 fluorescent lamps using intensity in the range of 0.71 W/m2. Samples were exposed uninterrupted, 24 h per day during 21 days.

Mechanical properties of the degraded surface of the PMMA/PU and PMMA/PU/$CePO_4$ IPNs were evaluated using an Anton Paar Nanoindentation Tester NHT3 with a Berkovich diamond indenter, equipped with the Indentation 7.2.5 software and using a linear loading/unloading rate of 100 mN/min and a max load of 5 mN.

3.0 Results and discussion.

3.1Study of compatibility by SEM and DSC of pure PMMA/PU IPNs

It has been well established that the detection of a single glass temperature transition (Tg) in polymer blends is indicative of their miscibility; while the detection **of two Tg** corresponding to their pure constituents indicates immiscibility [18]. Thus, to elucidate the compatibility of PMMA and PU forming the IPNs at different mixing times (10 and 60 min), DSC studies and SEM observations were performed on as-prepared samples. The thermograms and Tg values corresponding to PMMA, PU and PMMA/PU IPNs with the different weight ratios are displayed in Figure 1 and Table 1. No appreciable differences were acquired for the IPNs synthesized at 10 min and 1 h, and for that reason the thermograms corresponding to mixing time of 10 min were not included in the Figure (Figure III in supplementary material). Samples show only one intermediate Tg between pure PMMA (115 °C) and PU (148 °C) indicating that there is no phase separation after the polymerisation process, and that there is adequate compatibility between the two polymers in the synthesized samples. The only remarkable difference by comparing the mixing time was observed in samples with a

50:50 composition where the Tg was shifted from 138 °C to 156 °C, with 10 min and 60 min, respectively; which reflects the influence of the mixing time on the degree of interpenetration [19]. The mismatch in the temperatures is evidence of restricted chain mobility due to the better entanglement between PMMA and PU, i.e. with higher mixing times, PMMA has the opportunity to interlock in the continuous elastomeric domains (PU) that results in a decrease of free volume [20].

SEM morphologies of as-prepared PMMA/PU IPNs using both mixing times are shown in Figure 2 c-j.

For comparison, the figures 2a-b also show morphologies of the pure PMMA and PU. Similar morphologies independent of the mixing time are presented in 80/20 and 70/30 PMMA/PU IPNs. As it is seen in Figure 2c-f, these types of morphologies consist of homogeneous smooth surfaces which did not resemble the pure PMMA structure in Figure 2a. By comparing 10 min of mixing time in blends with higher amounts of PU (PMMA/PU 50/50 and 60/40) to those of 60 min, the homogeneity is seen as proof of their miscibility. The morphology for samples mixed for a short time (10 min) showed non-homogeneous textures consisting of dispersed nodular phase domains of few micrometres (**Figure 2 g and i**). These results indicate that from amounts of 40 wt.% of PU, the mixture needs more time to reach homogeneity. This feature has been reported in neat thermosets specimens [21] and it has been related to opacity and phase separation in polymers [22].

In contrast, PMMA/PU 50/50 and 60/40 (60 min) displayed a more homogeneous material and an interlocked morphology (Figure 2i and j) regardless of mixing time.

The more interlocked morphology in PMMA/PU 50/50 (Figure 2j) corroborates the DSC studies, where the increasing in the Tg was observed at the highest mixing time. After analysis of the mixing time, 60 min of mixing time was chosen for further analysis in pure PMMA/PU IPNs.

3.2 Structure and optical properties of $CePO_4$ nanostructures

The structure and TEM micrographs of $CePO_4$ nanostructures with their corresponding selected area electron diffraction (SAED) patterns are shown in Figure 3. Nanosized polycrystals and monocrystals of $CePO_4$ with semi-spherical and rod type-morphologies, both with monoclinic structure (PDF # 04-007-2786), were detected in samples synthesised at pH 11 and 1, respectively. It is important to highlight that the

chemical composition of these nanostructures was verified by X-ray photoelectron spectroscopy (Figure IV, see supplementary material).

Similarly, the emission spectra of each sample were studied using fluorescence measurements. Figure 4 shows the photoluminescence spectra of nanorods and semi-spherical nanoparticles, which were excited at 405 nm. The spectrum of nanoparticles with rod type morphology exhibits two characteristic emission peaks associated with $CePO_4$, one is located at 480 nm and 580 nm. In contrast, semi-spherical particles display a broad emission centred at 468 nm. These signals are attributed to 2F ➔ 2D transitions of Ce3+ ions [17, 23].

3.3 Structural changes during incorporation of $CePO_4$ to IPNs

FT-IR analysis has been performed to confirm the chemical structure of the PMMA/PU IPNs before and after the addition of $CePO_4$ (Figure 5a-d). As expected, FT-IR spectra in Figure 5a-d are characterized by the typical absorption bands of PMMA and PU single polymers [24-28].

There was no evidence of new vibrational bands indicating that as expected no new bonds were present since IPNs are only entangled and interlocked on molecular scale [29]. Typical bands of PMMA and PU are listed in Table 2 and 3.

$CePO_4$ absorption bands could not be detected in the spectra due to the low content added in IPNs (0.1 wt.%). **Donor-acceptor interaction between the electron pair of carbonyl oxygen and Ce^{3+} ion probably plays the main role in the stabilization of the $CePO_4$ nanostructures. Additionally, Ce nanostructures can interact with the vibrational C=O bands that appears in the 1716- 1650 cm^{-1} region**. **In tis important to note that C=O band was shifted to lower wavenumbers upon the addition of semi-spherical nanoparticles. This displacement indicates that apparently the higher surface area influences on the physical interactions and also, that the energy required to vibrate the C=O groups is higher (High frequency) when they interact with semi-spherical particles rather than rod-like (low frequency), which indicates the strong donor-acceptor interaction between them. Interactions between the hydrogen of the free N-H groups with the oxygen in $CePO_4$ and the electron pair of the nitrogen in PU with the cerium ions are other probable interactions [30]. A representation of the possible interactions is given in Figure 6. These interactions were proposed from the crystallographic planes observed during TEM analysis. The interaction of nanorods with**

PMMA/PU IPNs takes place preferentially on the high-energy exposed facets, such as (002) or (003) planes; it means that the interaction with the polymer is most probably with the oxygen contained in $CePO_4$ nanostructures rather than the cerium or phosphorous ions.

The interfacial non-covalent interaction was confirmed by analysing the carbonyl band by adding higher amounts of both type of morphology in PMMA/PU 50/50 IPN (Figure 5d). As it is observed, a broad band is detected in the 1770-1660 cm^{-1} region in samples containing 0.1 wt.%, independent of the morphology type. With further addition of semi-spherical nanostructures (0.5 and 1 wt.%), the carbonyl bands split into two separate well defined peaks designated as PMMA carbonyl (higher wavenumber) and PU carbonyls (lower wavenumber), respectively [31]. Thus, by adding more nanoparticles into the PMMA/PU IPN, we can distinguish both carbonyls that are interacting with the nanoparticles in the IPNs.

3.4 Optical properties

The degree of transparency and the influence of the 0.1, 0.5 and 1 wt.% of $CePO_4$ in 50/50 and 80/20 added to the PMMA/PU systems was evaluated by visible spectroscopy in the 400-700 nm range **which was considered as a gauge of optical properties. However, it is important to highlight that the percentage of the transmitted light that is able to pass through a material, it is not the only parameter that must be considered to analyse the optical properties; so it must be taken into account the percent of transmitted light that is scattered (> 2.5° from the direction of the incident beam). In such conditions, optical properties can be more properly determinate using haze measurements [32].**

Transmission spectra in the visible region for 50/50 and 80/20 ratio of PMMA/PU/$CePO_4$ IPNs are shown in Figure 7. Due to an increasing in light scattering, the incorporation of $CePO_4$ nanoparticles modifies the transmittance in the visible region [33],

It was observed that the addition of 0.1 wt.% of semi-spherical particles results in a higher transmittance than the addition of nanorods in 50/50 and 80/20 system. Another observation was that the transmittance was reduced as the content of $CePO_4$ increased in IPNs in both 50/50 and 80/20 systems. These observations agree with the visual observations in samples showed in Figure V in supplementary material where opaque samples are seen with higher wt.% of nanostructures. **Light scattering is undesirable in this type of polymers, as it can decrease the fraction of light absorbed [34].** As known, to maintain the transparency of a material, particles to be dispersed therein must be nanoparticles that scatter light only slightly

and this can be achieved by having no agglomeration of the nanoparticles **[35, 36]. Thus, the addition of $CePO_4$ nanostructures interferes with common degradation pathways in PMMA photochemistry. The reduction in transmittance of $CePO_4$ incorporation is affected by the particle size and morphology. For example, nanorods due to their anisotropic characteristics scatter light into different directions and this affect the appearance in the PMMA/PU systems producing opaque samples. On the other hand, semi-spherical nanoparticles, reflect light to a constant direction and produce a glossy appearance [37].**

3.5 Distribution of nanostructures in PMMA/PU IPNs.

3.5.1 CLSM and SEM/EDS

Some studies have shown the incorporation of different types of inorganic phases, however, $CePO_4$ nanoparticles have not been studied into interpenetrating polymer networks. Dispersion is one of the main factors that influence on the final properties. For many applications that includes high transmittance in visible light of materials, these nanoparticles would benefit from having $CePO_4$, in both morphologies, to impart structural and mechanical properties **as well as prolongation of** the lifetime.

A common technique to evaluate the dispersion of $CePO_4$ nanoparticles in PMMA/PU IPN systems is confocal laser scanning microscopy (CLSM). The technique allows us to identify the nanoparticles by detecting the wavelength of emission and generates images pixel by pixel while the sample is irradiated with UV light (in this study) [38].

In an attempt to compare the dispersion of the nanorods from the results of CLSM micrographs/spectra to those with semi-spherical nanostructures, we selected samples of PMMA/PU/ IPNs with $CePO_4$ nanoparticles dispersed at 0.1 wt.%.

Nanorods were incorporated homogenously in PMMA/PU 50/50 and 80/20 systems while the presence of agglomerates can be noticed in the images of the intermediate PMMA/PU IPNs ratio (60/40 and 70/30) (Figure 8).

The distribution of semi-spherical (Figure 9) in the IPNs showed that these nanostructures can be homogenously incorporated in the 60/40 ratio. However, the tendency to form agglomerates is more prevalent in 70/30 and 80/20 systems. For more clarity, different images of CLSM are included in Figure VI-VII in supplementary material.

The upconverting emission spectra of the selected samples are also shown in Figure 8 and 9. The results indicates that emission intensity tend to increase with the amount of PMMA in the hybrid system. Three main emission bands in the visible region can be observed 425-490 nm, 493-558nm, 562-625 nm which overlapped with the peaks associate with $CePO_4$ nanostructures. A small fluorescence emission is also observed in the region of 623-700 nm which could be associated with the used sources; PMMA/PU, photoinitiator, and/or $CePO_4$ nanostructures. In this work was used type I photoinitiator to start IPNs polymerization, which acts directly on PMMA. According to Liu and co-workers, the emission spectra of 1-hydroxycyclohexyl phenyl ketone (HPK) appears in the range of 420-450 nm, which surely overlaps in the region of 425-490 nm. On the other hand, a quite weak emission was observed in the $CePO_4$, therefore it seems to be evident that the main contribution of the emission at 623-700 nm belonged to the interpenetrating polymer network. The upconverting emission of the as-prepared samples suggest that the PMMA/PU/$CePO_4$ IPN nanohybrids can mantain the initial optical properties of PMMA [39] .

Comparison between the ratio of PMMA/PU and type of morphologies indicates that both types of morphologies are well dispersed in IPNs with less amount of PMMA (50/50 and 60/40). Nevertheless, comparison between nanorods and semi-spherical at the highest ratio with PMMA (80/20) indicates that nanorods are easier to disperse than semi-sphericals which may result from the high stiffness of the carbonyls C=O and methyl groups (CH_3) in PMMA macromolecule and the tendency of nanorods type that tend to have lowest surface specific area than semi-spherical.

In an effort to get a better understanding of dispersion/distribution of the different wt.% of $CePO_4$ in PMMA/PU IPNs, samples with the highest and lowest ratio of PMMA/PU (80/20 and 50/50) were selected to acquire EDX mapping images. Results are shown in Figure 10. The results are presented as yellow dots of the cerium (the element of interest) in samples, also SEM micrographs are shown as inset figures.

$CePO_4$ nanostructures were found to be more difficult to disperse in samples with high PMMA content. The reason that the nanoparticles are well dispersed in a 50:50 ratio is related with compatibility of the polymers forming the IPNs. As it is being stated, an excess of PMMA produces a system completely phase separated [7]. Then, this produces that polyurethane at 20 wt.% of addition cannot be fully interlocked with the PMMA; consequently, it is probable that the phases were slightly separated and this avoids the

incorporation of the nanostructures in the free sites of the IPNs and their physical interaction with the carbonyls groups.

The inset micrographs also show that IPNs with an excess of PMMA display the typical coarse morphology of PMMA (Figure 2a) and thermoset materials [21]. On the other hand, with the addition of 50 wt.% of PU, PMMA/PU 50/50 showed a smooth texture similar to pure PU (Figure 3b).

Another observation was the amount (wt.%) of nanoparticles added to the systems. It was seen that independent of the morphology type, the $CePO_4$ nanoparticles dispersed at the lowest amount (0.1 wt.%) were distributed uniformly in the 50/50 and 80/20 PMMA/PU IPNs. However, higher amounts of $CePO_4$ (0.5 and 1 wt.%) into PMMA/PU caused the formation of some agglomerates which is dots over the surface of the micrographs. The latest can be clearly observed when the nanorods are added in an 80/20 ratio.

3.5.2 Surface properties

Water sessile drop contact angle tendencies are shown in Figures 11. As it is shown, the water contact angle (C.A.) for pure samples in 50/50 and 80/20 ratios showed values c.a. 80° and 85°, respectively. These results are higher to the neat PMMA reported in different reports [40-43] and in good agreement with previous research where a water contact angle of c.a. 81° was reported for PMMA/PU (tolylene-2,4-diisocyanate, TDI) system [8].

It is known that in rare earth phosphate systems, the H_2O repelling nature is explained based on one-way H-bond interactions between the H+ of water and O- of the $\boldsymbol{PO_4^{3-}}$ moieties [44]. The bulky $\boldsymbol{PO_4^{3-}}$ units surrounding the ions can make them available for interacting with H_2O. In this case, the addition of both type of nanostructures of $CePO_4$ unfortunately did not improve the wettability properties showing C.A. between 80-89°.

3.5.3 Thermal properties

DSC thermograms of every ratio of PMMA/PU with the addition of the nanostructures in varying wt.% are compared in Figure 12. Quantitative results obtained from DSC are presented in Table 1.

It was seen that independent of the morphology and the wt.% added (semi-spherical or rod), the addition of $CePO_4$ in the 80/20 system of PMMA/PU IPNs did not produce an important change in the Tg since the values obtained (124 °C) are near to the Tg of pure 80/20 IPN (123

°C). On the other hand, the Tg of pure PMMA/PU 50/50 is modified dramatically when nanorods are added since it is reduced from 148 °C (pure 50/50 IPN), to 124 °C, 123 °C and 120 °C. As stated in previous reports, the Tg of polymer nanocomposites can be modulated by polymer-nanofiller interactions [45]. Hydrogen bonds is an example of effects that can lead to enhancements rather than depression in **Tg** [46]. A reduction in Tg has been reported due to weak interactions between filler and polymer [47].

As can be seen from the data above, these types of nanostructures did not increase the Tg and the reduction could be due to the plasticizer effect of these nanoparticles which are similar to the POSS-polymer surface interactions with isobutyl (iBu) systems [48]. However, it was observed that the Tg of 50/50 IPNs with semi-spherical particles is maintained between 123-124 °C.

An interesting observation in the DSC thermograms was observed with the appearance of new endothermic processes in almost all of the PMMA/PU IPNs upon the addition of the nanostructures. These endothermic peaks are attributed to the structural relaxation process that arise from the molecular rearrangement in the structure as a consequence of the reduction of free volume, well known as densification [49].

The incorporation of nanorods apparently produces one **relaxation peak, whereas** the addition of semi-spherical particles produces overlapped peaks consisting of two signals close each other. Recovery peaks have been used to explore the miscibility of polymer blends. For example, miscible PMMA/PVC blends display a single peak, indicating a one-phase system that is miscible [50]. However, interpenetrating polymer networks are heterogeneous systems forced by entanglement and are different from miscible polymer blends [51]. Therefore, the appearance of recovery peaks is due to the heterogeneous systems as interpenetrating polymer networks. These peaks represent the recovery of energy relaxed; larger peaks signify greater structural relaxation [52].

In order to evaluate the recovery of energy relaxed, the area under the peaks was calculated and is shown in Table 1. It was observed that heat flow of relaxation increases with the amount of nanostructures (both) and there is a shifting to higher temperatures in 50/50 systems.

In 80/20 systems with nanorods incorporated, the heat flow of peaks decreases with the 0.1 and 0.5 wt.% of nanostructures but increases with the addition of 1 wt.% which consists of two relaxation peaks; in this case the temperature is shifted to lower values. This was also seen upon the addition of these semi-spherical particles. In nanocomposites, the phenomenon

of increasing relaxation peak is indicative of the increasing temperature range required to increase the mobility of the polymer chains ([53]).

TGA curves of PMMA and PU in Figure 13a showed single and double stage degradation and no mass loss up to 240 °C and 310 °C, respectively indicating good thermal stability up to those temperatures.

The PMMA derivative curve in Figure 13c display three peaks corresponding to the CO_2 and CO vapours (320 °C), the chain breaking of the carbonyl groups located in the surrounding of the cross-linking points as well as of the degradation of the acrylate groups (380 °C) and decomposition of crosslinking agent fragment (435 °C) [54, 55].

In the case of PU, the DTGA curve also exhibits two stage of degradation at 386 °C and 425-437 °C; where the 1st stage is due to the breakdown of the urethane linkage to the polyol and isocyanate and the 2nd is due to the polyol and diisocyanate decomposition into small molecules (primary amine, alkene, aldehyde, ketone, carbon dioxide, water) [56, 57].

For all PMMA/PU IPNs, two stage thermal decomposition was observed. There is not much change in the thermal stability of selected PMMA/PU (80/20) with the incorporation of $CePO_4$ in both the rod and semi-spherical morphologies. However, the thermal properties of IPNs were found to be better than the single polymers.

3.5.4 Mechanical properties

Mechanical data and fracture optical images of PMMA/PU and PMMA/PU/$CePO_4$ IPNs are reported in Table 4, Figure 14 and Figure

VIII (Supplementary material). We investigated the effect of the different ratio of PMMA/PU and the addition of different wt.% (0.1, 0.5 and 1 wt.%) as well as the influence of morphologies (rod and semi-spherical).

As expected, the introduction of aliphatic PU led to significant changes in the mechanical properties. The effect of adding more than 20 wt.% of PU in PMMA was quite significant in the Young´s modulus, tensile strength and strain (%). The Young´s modulus was reduced together with tensile strength since to the toughness effect that the soft PU imparts to the rigid PMMA; strain (%) was increased satisfactorily from 124% (80/20 ratio) to 238 % (50/50 ratio).

The study of addition of different morphologies of $CePO_4$ in PMMA/PU IPNs gives an indication of the dispersion and its correlation to the shape (morphology of nanostructure) on the final mechanical properties. Both types of morphologies were found to improve the mechanical properties**; the** nanorods particularly increased the extensibility when there is less

amount of PMMA (50/50). On the contrary, semi-spherical particles increase the deformation percent when PMMA is in higher amounts (80/20). This increase is mainly **to the** ductile character of $CePO_4$ which was reported earlier by W. Lijuan **et al.** [58].

As is observed in the Young´s modulus results, the addition of only 0.1 wt.% of nanorods reduces the stiffness of the pure matrix from 7 MPa to value of 2.37 MPa, it was observed that with this wt.% the % of strain was improved significantly (856%) while maintaining a similar the tensile strength to the pure matrix. This behaviour in strain (%) and Young modulus is restricted to the wt. % of the addition; if they are added in higher amounts (>0.5 wt.%), samples become more rigid than the hybrid with 0.1% but less than the pure matrix. Therefore, the extensibility is reduced by increasing the content (wt.%) added, 761 % and 652 % for 0.5 % and 1 wt.%, respectively.

The study of incorporation of semi-spherical particles indicates that this types of nanostructure can also improve the mechanical properties of pure PMMA/PU 50/50 IPN but not significantly as the incorporation of 0.1 wt.% of nanorods. Samples display Young modulus c.a. 3 MPa, tensile strength between 54-30 MPa and % of strain of 323-654 % which increases with the amount of semi-spherical nanoparticles.

The incorporation of nanorods in 60/40 system also decreased the Young´s modulus slightly and reduced the tensile strength compared to the pure matrix; in this case, the increase in tensile strength and extensibility is improved with the amount of nanostructures. In contrast, the incorporation of semi-spherical particles reduced the Young modulus further than the addition of nanorods, displayed improved tensile strength behaviour and reached strains of up to 975 % (obtained by only adding 0.1 wt.% which is decreased with the amount of semi-spherical (760-864 %)).

It was observed that nanorods in the different % of addition (0.1, 0.5 and 1 wt.%) in 70/30 system display similar Young modulus and strain, however, sample with 0.1 wt.% show low tensile strength than the others. On the other hand, the addition of semi-spherical type (0.1 wt.%) has the same behaviour as nanorods. The addition of more than 0.5 wt.% increase the stiffness (higher Young modulus) and the tensile strength, however only the addition of 0.5 wt.% improve the extensibility until 452 %.

In general, young modulus of IPNs with a higher amount of PMMA (i.e., PMMA/PU 80/20 IPN) were reduced by incorporating either nanorods or semi-spherical nanostructures.

The introduction of nanorods did not improve significantly the **Young's** modulus but increased the tensile strength with the wt.% of nanostructures (27, 24 and 35 MPa for 0.1, 0.5 and 1 wt.%, respectively). Strain (%) of pure matrix with the nanorods is maintained between

122-141 %, except for the sample with 0.5% that showed 78% of extensibility; this value could probably be due to the not well dispersion of the nanoparticles in 80/20.

On the contrary to the nanorods, better ductility is provided by adding only 0.1 wt.% (722%), this system (80/20) is characterized by lower Young´s modulus (6.9 MPa) and higher tensile strength (39 N) than the pure matrix. The addition of more than 0.5 wt.% increased the stiffness (high Young´s modulus) and reduces the tensile strength and extensibility proportionally.

As it was observed, integration of $CePO_4$ nanostructures in rod and semi-spherical morphology in PMMA/PU IPN provides excellent mechanical properties. Most notably, these systems are better in Young´s modulus, in tensile strength and strain than other similar systems reported for pure PMMA/PU IPNs [7].

Despite the improvement in mechanical properties, the homogeneity of the dispersion of nanoparticles in the nanocomposites is still debated [59], we believe that the different value in mechanical properties, mainly the strain, is mainly due to the degree of dispersion of semi-spherical and rods nanostructures. It is obvious that the addition of 0.5 and 1 wt.% is more difficult than 0.1 wt.%; we know that nanostructures have largest surface specific area that leads to higher degree of agglomeration, this makes them more difficult to disperse into the polymer matrix IPN[60]. We do believe that if nanorods in 0.5 wt.% and 1 wt.% in 50/50 and 80/20 were more dispersed, the mechanical properties such as the extensibility could go higher than 856 % and 722%, respectively.

Another interesting observation of this study was the influence of the amount of the type of polymer (PU or PMMA). Overall, when there is a lower amount of PMMA, both type of morphologies were found to increase the mechanical properties and with more PMMA, mechanical properties are lower. The latter was observed in sample with 0.1 wt.% (semi-spherical) that it was easier to incorporate and disperse and produce results compared to the PMMA/PU/$CePO_4$ nanorods hybrids.

Therefore, enhancements in strength, elongation and Young's modulus might be attributed to the homogeneous dispersion and the interfacial bonding between the organic polymer and inorganic $CePO_4$ nanoparticles in the nanocomposites.

3.5.5 Heat and humidity aging

To better understand the mechanical stability under heat and humidity conditions and the consequences on the mechanical properties of selected PMMA/PU and PMMA/PU/$CePO_4$, IPNs were evaluated by tensile testing after 500 h of accelerated aging. It is evident that

polymeric materials undergo degradation under these conditions, therefore their mechanical performances will progressively decrease with time [61]. As it is shown in Table 5, elongation at break, tensile strength and Young´s modulus of all samples showed a detriment in mechanical properties after aging. Samples in 50/50 and 80/20 ratio of PMMA/PU with 0.1 wt.% of semi-spherical type $CePO_4$ nanoparticles showed the best stability under aging. Compared to $CePO_4$ semi-spherical type, the addition of the same % of nanorods did not maintain the stability after 500 h probably due to the dispersion of bigger particles. As it was mentioned above, nanorods were found **to be easier** to disperse than semi-spherical. Therefore, if the latest in higher wt.% of addition, were well dispersed, they would maintain the mechanical properties and prolong the lifetime under thermal (60 °C) and humid conditions. No significant damage such as cracking was observed on the aged samples (Figure IX, See supplementary material).

3.5.6 Accelerated weathering test (UV light)

Mechanical properties of selected PMMA/PU/$CePO_4$ IPNs were evaluated before and after of being subjected to accelerated weathering test (using UV light and humidity) by nanoindentation test. Instrumental hardness and elastic modulus of selected aged and non-aged PMMA/PU/$CePO_4$ IPNs were determinate from the load-unloading curves by using the following formulas:

$$H_{IT} = \frac{F}{A(h_c)}$$

$$E_{IT} = \frac{(1 - v_{IT}^2)}{\left\{\frac{2}{\sqrt{\pi}} \frac{\sqrt{Ah_c}}{S} - \frac{(1 - v_{indenter}^2}{E_{indenter}}\right\}}$$

Where A(hc) is the projected contact area which is calculated by knowing the geometry of the nanoindenter and the contact hardness. v_{IT} **is the ratio of Poisson,** $v_{indenter}$ is the ratio of Poisson of indenter, S is the slope of the tangent of the force/indentation during unloading curve and hc is the depth of contact which depends on the shape of indenter. It is important to note that measurement of elastic modulus acquired from nanoindentation and tensile test do not correlate exactly due to the different effects such as surface effects, surface oxidation, type of loading is compressive in nanoindentation (not tensile), etc [62]. **Therefore,** these values cannot be compared to those of the Young´s modulus obtained from the tensile test.

In Table 6 the variation of HIT and EIT of the unexposed and exposed surfaces of selected samples is shown. In the case of pure IPNs in 80/20 and 50/50 ratio, it was not possible to

analyse the HIT and EIT since samples were found broken after aging, as shown in Figure X in supplementary material, samples became rigid and cracked due to the degradation.

The differences of the UV/humidity stability between the addition of semi-spherical and nanorod was evaluated in 80/20 systems. In this case, the HIT and EIT increased from 1.3 to 3.2 GPa with the addition of nanorods while with semi-spherical, the mechanical properties were maintained. This was confirmed with increasing the values in 50/50 system with the addition of semi-spherical particles. As it is stated, polymers subjected to accelerated weathering tends to increase the stiffness and the Young´s modulus due to the alternation of wet/dry and the damage of UV light which produces crosslinking reactions [63]. Some mechanisms suggest that the increasing of elastic modulus is due to the physical aging (no chemical modification), to the difference between room temperature and Tg increases [64], to the hydrogen bonding generated after aging and the additional cross-linking leading to increase the structural network density since new bonds can be generated between the existing chain segments or between the chains. Therefore, cross-linking leads to harder materials, characteristics of high EIT and HIT [62, 63].

In summary, $CePO_4$ nanostructures can mechanically strengthened PMMA/PU interpenetrating polymer networks while supress the typical PMMA photodegradation. It is well known that PMMA photolysis involves the triplet carbonyl and O_2 triggered from the formation of oxidizing reactive species via Norrish type reactions. $CePO_4$ nanostructures avoid irreversible damage caused by photocleavage of the polymers (Norris type I) and photooxidation acting as light quenching [15, 65, 66].

4. Conclusions

As illustrated by the different studies done in this work, prolongation of lifetime of interpenetrating polymer networks (IPNS) composed of PMMA/PU can be improved by incorporating cerium phosphate nanoparticles with either nanorod or semi-spherical type morphology. Our observations suggest that pure PMMA/PU IPNs did not maintain their final properties under UV light due to the absorption of them in this range. In fact, samples became cracked and damaged (Figure 15). But, when $CePO_4$ nanoparticles are incorporated, they can absorb the energy in this range and be excited; electrons in valence band can jump up to higher energy states releasing their energy into a lower energy in the visible range where PMMA/PU are invisible and the released photons cannot damage at all the polymers. **Semi-sphericals** more than nanorods have a better performance in the lifetime of PMMA/PU/$CePO_4$ which is mainly due to the type of morphology.

An improvement in the lifetime and mechanical properties of PMMA was achieved by the incorporation of upconverting $CePO_4$ luminescent nanoparticles and PU in different wt.% prepared by the sequential polymerisation of PMMA/PU. The resulting PMMA/PU/$CePO_4$ hybrid material prepared not only possess adequate optical and mechanical properties, it also exhibits structural, wettability and thermal properties for outdoors applications.

The final properties of PMMA/PU/$CePO_4$ depend on the dispersion and the morphology type. Nanorods were more easily dispersed than semi-spherical particles due to their low specific area, and contributed to an increase the strain due to the nanorods orientation. However, when semi-spherical are better dispersed, they can provide and maintain the properties after being subjected to accelerated weathering essays either by using heat/humidity or UV radiation/humidity/heat.

Acknowledgements

D. Palma-Ramírez is grateful for her postgraduate fellowship to CONACYT, COFAA and SIP-IPN. Authors would like to thank to Loughborough Materials Characterisation Centre (LMCC), especially to Dr. Keith Yendall and Dr. Zhaoxia Zhou for their technical support and research assistance with this project. The authors are also grateful for the financial support provided by Instituto Politécnico Nacional through the SIP 2017-1186, and COFAA; CONACYT through the CB-20151320 and SNI-CONACYT.

REFERENCES

[1] S. Fuina, G.C. Marano, G. Puglisi, D. De Tommasi, G. Scarascia-Mugnozza, Thermo-mechanical response of rigid plastic laminates for greenhouse covering, 2016 47(3) (2016) 7.
[2] J.A. Strauss, P.A. Soave, R.S. Ribeiro, F. Horowitz, Absorber and self-cleaning surfaces on modified polymer plates for solar harvesting in the humid (sub)tropics, Solar Energy 122 (2015) 579-586.
[3] S.M. El-Bashir, F.F. Al-Harbi, H. Elburaih, F. Al-Faifi, I.S. Yahia, Red photoluminescent PMMA nanohybrid films for modifying the spectral distribution of solar radiation inside greenhouses, Renewable Energy 85 (2016) 928-938.
[4] C. Indermühle, E. Puzenat, F. Simonet, L. Peruchon, C. Brochier, C. Guillard, Modelling of UV optical ageing of optical fibre fabric coated with TiO2, Applied Catalysis B: Environmental 182 (2016) 229-235.
[5] J. David, R. Hayes, J. Hui, R. Nay, Nanoindentation as an alternative to mechanical abrasion for assessing wear of polymeric automotive coatings, Journal of Coatings Technology and Research 13(4) (2016) 677-690.

[6] M.S. Um, D.S. Ham, S.K. Cho, S.-J. Lee, K.J. Kim, J.H. Lee, S.-H. Choa, H.W. Jung, W.J. Choi, Surface mechanical properties of poly(urethane acrylate)/silica hybrid interpenetrating polymer network (IPN) coatings, Progress in Organic Coatings 97 (2016) 166-174.
[7] K.C. Jajam, S.A. Bird, M.L. Auad, H.V. Tippur, Tensile, fracture and impact behavior of transparent Interpenetrating Polymer Networks with polyurethane-poly(methyl methacrylate), Polymer Testing 32(5) (2013) 889-900.
[8] W.S.Y. Wong, Z.H. Stachurski, D.R. Nisbet, A. Tricoli, Ultra-Durable and Transparent Self-Cleaning Surfaces by Large-Scale Self-Assembly of Hierarchical Interpenetrated Polymer Networks, ACS Applied Materials & Interfaces 8(21) (2016) 13615-13623.
[9] S.S. Ray, M. Bousmina, A. Maazouz, Morphology and properties of organoclay modified polycarbonate/poly(methyl methacrylate) blend, Polymer Engineering & Science 46(8) (2006) 1121-1129.
[10] J.-M. Widmaier, G. Bonilla, In situ synthesis of optically transparent interpenetrating organic/inorganic networks, Polymers for Advanced Technologies 17(9-10) (2006) 634-640.
[11] T. Phuttachart, N. Kreua-ongarjnukool, R. Yeetsorn, M. Phongaksorn, PMMA/PU/CB Composite Bipolar Plate for Direct Methanol Fuel Cell, Energy Procedia 52 (2014) 516-524.
[12] T. Dongyan, L. Hong, C. Weimin, synthesis and application studies of castor oil PU/PMMA IPNs with BaTiO3 fiber nanocomposites, Ferroelectrics 265(1) (2002) 259-264.
[13] T. Jeevananda, Siddaramaiah, Synthesis and characterization of polyaniline filled PU/PMMA interpenetrating polymer networks, European Polymer Journal 39(3) (2003) 569-578.
[14] T. Dongyan, Q. Liangsheng, J. Zheng, C. Weimin, Preparation, morphology, and thermoelectric property studies of BaTiO3 superfine fiber/castor oil polyurethane-based IPN nanocomposites, Journal of Applied Polymer Science 84(4) (2002) 709-715.
[15] J.F. De Lima, O.A. Serra, Cerium phosphate nanoparticles with low photocatalytic activity for UV light absorption application in photoprotection, Dyes and Pigments 97(2) (2013) 291-296.
[16] D. Palma-Ramírez, M.A. Domínguez-Crespo, A.M. Torres-Huerta, H. Dorantes-Rosales, E. Ramírez-Meneses, E. Rodríguez, Microwave-assisted hydrothermal synthesis of CePO4 nanostructures: Correlation between the structural and optical properties, Journal of Alloys and Compounds 643 (2015) S209-S218.
[17] N. Ekthammathat, T. Thongtem, A. Phuruangrat, S. Thongtem, Facile hydrothermal synthesis and optical properties of monoclinic CePO4 nanowires with high aspect ratio, J. Nanomaterials 2012 (2012) 1-6.
[18] H. Bourara, S. Hadjout, Z. Benabdelghani, A. Etxeberria, Miscibility and Hydrogen Bonding in Blends of Poly(4-vinylphenol)/Poly(vinyl methyl ketone), Polymers 6(11) (2014) 2752.
[19] C. Rocco, F. Karasu, C. Croutxé-Barghorn, X. Allonas, M. Lecompère, G. Riess, Y. Zhang, A.C.C. Esteves, L.G.J. van der Ven, R.A.T.M. van Benthem, G. de With, Highly-interpenetrated and phase-separated UV-cured interpenetrating methacrylate–epoxide polymer networks: Influence of the composition on properties and microstructure, Materials Today Communications 6 (2016) 17-27.
[20] H. Kaczmarek, I. Vukovic-Kwiatkowska, Preparation and characterization of interpenetrating networks based on polyacrylates and poly(lactic acid), eXPRESS Polymer Letters 6(1) (2012) 89-94.
[21] M. Sangermano, W.D. Cook, S. Papagna, S. Grassini, Hybrid UV-cured organic–inorganic IPNs, European Polymer Journal 48(10) (2012) 1796-1804.

[22] J. Laskar, F. Vidal, O. Fichet, C. Gauthier, D. Teyssié, Synthesis and characterization of interpenetrating networks from polycarbonate and cellulose acetate butyrate, Polymer 45(15) (2004) 5047-5055.
[23] H. Yang, L. Yuan, G. Zhu, A. Yu, H. Xu, Luminescent properties of YAG:Ce3+ phosphor powders prepared by hydrothermal-homogeneous precipitation method, Materials Letters 63(27) (2009) 2271-2273.
[24] D.K. Chattopadhyay, B. Sreedhar, K.V.S.N. Raju, The phase mixing studies on moisture cured polyurethane-ureas during cure, Polymer 47(11) (2006) 3814-3825.
[25] A. Balamurugan, S. Kannan, V. Selvaraj, S. Rajeswari, Development and Spectral Characterization of Poly(Methyl Methacrylate) /Hydroxyapatite Composite for Biomedical Applications, Trends Biomater. Artif. Organs 18(1) (2004) 41-45.
[26] B.H. Stuart, Spectral Analysis, Infrared Spectroscopy: Fundamentals and Applications, John Wiley & Sons, Ltd2005, pp. 45-70.
[27] G. Duan, C. Zhang, A. Li, X. Yang, L. Lu, X. Wang, Preparation and Characterization of Mesoporous Zirconia Made by Using a Poly (methyl methacrylate) Template, Nanoscale Research Letters 3(3) (2008) 118-122.
[28] J.M. O'Reilly, R.A. Mosher, Conformational energies of stereoregular poly(methyl methacrylate) by Fourier transform infrared spectroscopy, Macromolecules 14(3) (1981) 602-608.
[29] Y. Gong, X. Liao, J. Xu, D. Chen, H. Zhang, Novel anion-conducting interpenetrating polymer network of quaternized polysulfone and poly(vinyl alcohol) for alkaline fuel cells, International Journal of Hydrogen Energy 41(13) (2016) 5816-5823.
[30] H. Liu, P. Bandyopadhyay, N.H. Kim, B. Moon, J.H. Lee, Surface modified graphene oxide/poly(vinyl alcohol) composite for enhanced hydrogen gas barrier film, Polymer Testing 50 (2016) 49-56.
[31] Y.I. Tien, K.H. Wei, Hydrogen bonding and mechanical properties in segmented montmorillonite/polyurethane nanocomposites of different hard segment ratios, Polymer 42(7) (2001) 3213-3221.
[32] F.W. Billmeyer, Y. Chen, On the measurement of haze, Color Research & Application 10(4) (1985) 219-224.
[33] W. Caseri, INORGANIC NANOPARTICLES AS OPTICALLY EFFECTIVE ADDITIVES FOR POLYMERS, Chemical Engineering Communications 196(5) (2008) 549-572.
[34] N. Sekine, C.-H. Chou, W.L. Kwan, Y. Yang, ZnO nano-ridge structure and its application in inverted polymer solar cell, Organic Electronics 10(8) (2009) 1473-1477.
[35] T. Tadano, R. Zhu, Y. Muroga, T. Hoshi, D. Sasaki, S. Yano, T. Sawaguchi, A new mechanism for the silica nanoparticle dispersion–agglomeration transition in a poly(methyl methacrylate)/silica hybrid suspension, Polymer Journal 46 (2014) 342.
[36] T. Itoh, T. Uchida, N. Izu, I. Matsubara, W. Shin, Effect of Core–Shell Ceria/Poly(vinylpyrrolidone) (PVP) Nanoparticles Incorporated in Polymer Films and Their Optical Properties, Materials 6(6) (2013) 2119.
[37] T. Fukui, J. Tatami, S. Sakaguchi, F. Wakai, T. Senda, T. Akatsu, T. Baba, Y. Noguchi, M. Miyayama, A. Yamamoto, S. Yonezawa, T. Okamoto, M. Matsuda, M. Awano, T. Katamoto, K. Toda, S. Kirihara, A. Suda, K. Nogi, CHAPTER 6 - EVALUATION METHODS FOR PROPERTIES OF NANOSTRUCTURED BODY, Nanoparticle Technology Handbook, Elsevier, Amsterdam, 2008, pp. 317-383.
[38] J. Jonkman, C.M. Brown, Any Way You Slice It—A Comparison of Confocal Microscopy Techniques, Journal of Biomolecular Techniques : JBT 26(2) (2015) 54-65.
[39] T.-H. Liu, W.-T. Cheng, J.-J. Lin, Effect of Photo-initiator on Photosensitive Emission Polymer, Journal of Photopolymer Science and Technology 26(6) (2013) 757-764.

[40] M. Khayet, M. Vázquez Álvarez, K.C. Khulbe, T. Matsuura, Preferential surface segregation of homopolymer and copolymer blend films, Surface Science 601(4) (2007) 885-895.
[41] J. Wang, W. Zhou, J. Zhang, M. Yang, C. Ji, X. Shao, L. Shi, High-fidelity replica molding for large-area PMMA 3D nanostructures with high performance surface-enhanced Raman scattering and hydrophobicity, Microelectronic Engineering 115 (2014) 2-5.
[42] T. Coan, G.S. Barroso, R.A.F. Machado, F.S. de Souza, A. Spinelli, G. Motz, A novel organic-inorganic PMMA/polysilazane hybrid polymer for corrosion protection, Progress in Organic Coatings 89 (2015) 220-230.
[43] H.H. Tran, W. Wu, N.Y. Lee, Ethanol and UV-assisted instantaneous bonding of PMMA assemblies and tuning in bonding reversibility, Sensors and Actuators B: Chemical 181 (2013) 955-962.
[44] S. Sankar, B.N. Nair, T. Suzuki, G.M. Anilkumar, M. Padmanabhan, U.N.S. Hareesh, K.G. Warrier, Hydrophobic and Metallophobic Surfaces: Highly Stable Non-wetting Inorganic Surfaces Based on Lanthanum Phosphate Nanorods, Scientific Reports 6 (2016) 22732.
[45] B.J. Ash, L.S. Schadler, R.W. Siegel, Glass transition behavior of alumina/polymethylmethacrylate nanocomposites, Materials Letters 55(1–2) (2002) 83-87.
[46] P. Rittigstein, J.M. Torkelson, Polymer–nanoparticle interfacial interactions in polymer nanocomposites: Confinement effects on glass transition temperature and suppression of physical aging, Journal of Polymer Science Part B: Polymer Physics 44(20) (2006) 2935-2943.
[47] D. Fragiadakis, P. Pissis, L. Bokobza, Glass transition and molecular dynamics in poly(dimethylsiloxane)/silica nanocomposites, Polymer 46(16) (2005) 6001-6008.
[48] E. Ayandele, B. Sarkar, P. Alexandridis, Polyhedral Oligomeric Silsesquioxane (POSS)-Containing Polymer Nanocomposites, Nanomaterials 2(4) (2012) 445.
[49] H. Maljaee, B. Ghiassi, P.B. Lourenço, Effect of synergistic environmental conditions on thermal properties of a cold curing epoxy resin, Composites Part B: Engineering 113 (2017) 152-163.
[50] A.I. Isayev, Encyclopedia of Polymer Blends, Volume 1: Fundamentals, Wiley2016.
[51] J.R. Nair, M. Destro, F. Bella, G.B. Appetecchi, C. Gerbaldi, Thermally cured semi-interpenetrating electrolyte networks (s-IPN) for safe and aging-resistant secondary lithium polymer batteries, Journal of Power Sources 306 (2016) 258-267.
[52] S. Napolitano, Non-equilibrium Phenomena in Confined Soft Matter: Irreversible Adsorption, Physical Aging and Glass Transition at the Nanoscale, Springer International Publishing2015.
[53] N.A. Koratkar, Graphene in Composite Materials: Synthesis, Characterization and Applications, DEStech Publications, Incorporated2013.
[54] A. Vuillequez, J. Moreau, M.R. Garda, B. Youssef, J.M. Saiter, Polyurethane methacrylate/silicone interpenetrating polymer networks synthesis, thermal and mechanical properties, Journal of Polymer Research 15(2) (2008) 89-96.
[55] S.M. Lomakin, J.E. Brown, R.S. Breese, M.R. Nyden, An investigation of the thermal stability and char-forming tendency of cross-linked poly(methyl methacrylate), Polymer Degradation and Stability 41(2) (1993) 229-243.
[56] S.A. Shokry, A.K. El Morsi, M.S. Sabaa, R.R. Mohamed, H.E. El Sorogy, Synthesis and characterization of polyurethane based on hydroxyl terminated polybutadiene and reinforced by carbon nanotubes, Egyptian Journal of Petroleum 24(2) (2015) 145-154.
[57] V. Athawale, S. Kolekar, INTERPENETRATING POLYMER NETWORKS BASED ON OIL MODIFIED CASTOR OIL URETHANE AND POLY(METHYL METHACRYLATE), Journal of Macromolecular Science, Part A 37(1-2) (2000) 65-79.

[58] W. Lijuan, D. Haiyan, O. Xiujuan, Microstructure and properties of CePO4 ceramic, Journal of Wuhan University of Technology-Mater. Sci. Ed. 21(2) (2006) 120-122.
[59] S.F. Ferdous, M.F. Sarker, A. Adnan, Role of nanoparticle dispersion and filler-matrix interface on the matrix dominated failure of rigid C60-PE nanocomposites: A molecular dynamics simulation study, Polymer 54(10) (2013) 2565-2576.
[60] K. Suttiponparnit, J. Jiang, M. Sahu, S. Suvachittanont, T. Charinpanitkul, P. Biswas, Role of Surface Area, Primary Particle Size, and Crystal Phase on Titanium Dioxide Nanoparticle Dispersion Properties, Nanoscale Res Lett 6(1) (2010) 27.
[61] Z. Wang, X. Zhang, F. Wang, X. Lan, Y. Zhou, Effects of aging on the structural, mechanical, and thermal properties of the silicone rubber current transformer insulation bushing for a 500 kV substation, SpringerPlus 5(1) (2016) 790.
[62] P.N. Eleni, M.K. Krokida, G.L. Polyzois, C.A. Charitidis, E.P. Koumoulos, V.P. Tsikourkitoudi, I. Ziomas, Mechanical behaviour of a poydimethylsiloxane elastomer after outdoor weathering in two different weathering locations, Polymer Degradation and Stability 96(4) (2011) 470-476.
[63] M. Vlad-Cristea, B. Riedl, P. Blanchet, E. Jimenez-Pique, Nanocharacterization techniques for investigating the durability of wood coatings, European Polymer Journal 48(3) (2012) 441-453.
[64] A. Skaja, D. Fernando, S. Croll, Mechanical property changes and degradation during accelerated weathering of polyester-urethane coatings, JCT Research 3(1) (2006) 41-51.
[65] B.R. Anderson, R. Gunawidjaja, H. Eilers, Photodegradation and self-healing in a Rhodamine 6G dye and Y_2O_3 nanoparticle-doped polyurethane random laser, Applied Physics B 120(1) (2015) 1-12.
[66] T. Lippert, Interaction of Photons with Polymers: From Surface Modification to Ablation, Plasma Processes and Polymers 2(7) (2005) 525-546.

Figures

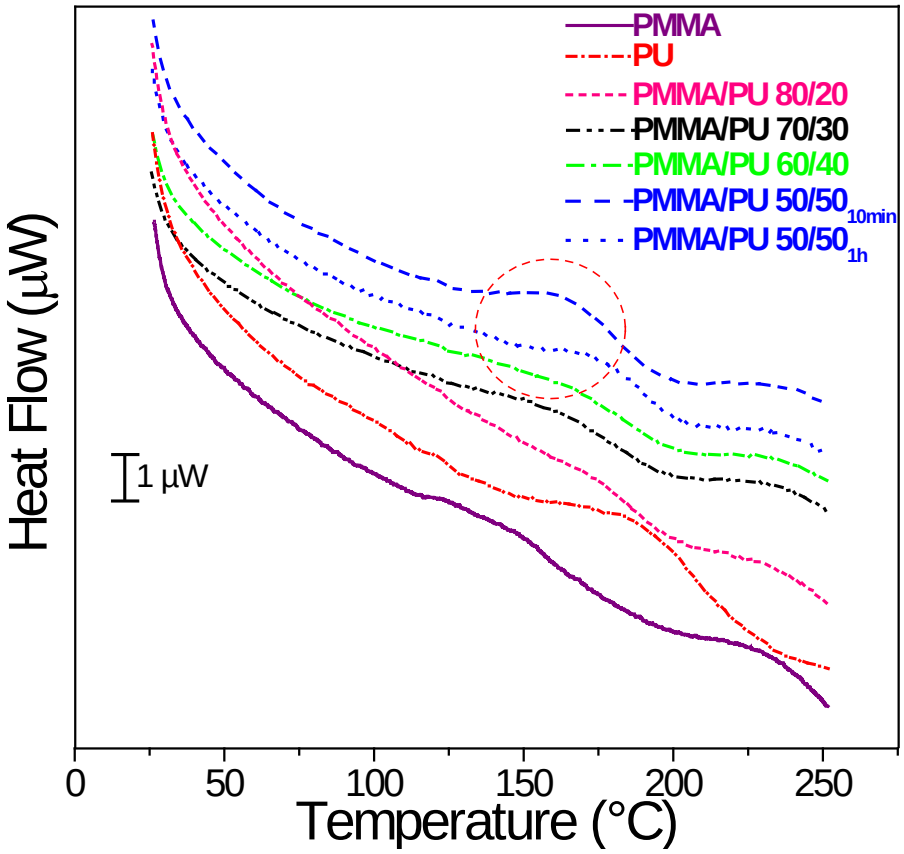

Figure 1. DSC thermograms of PMMA, PU and pure PMMA/PU IPNs

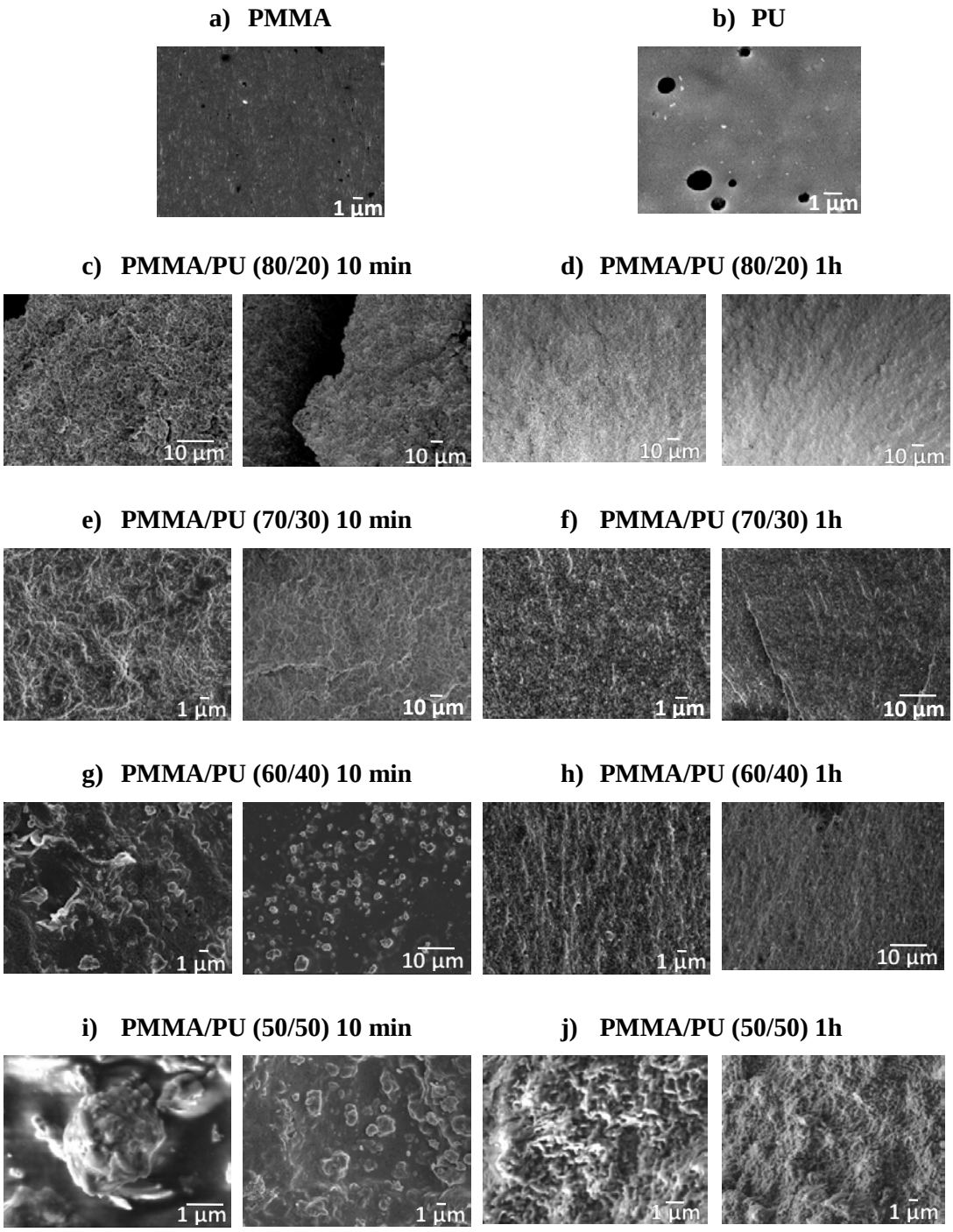

Figure 2. SEM micrographs of the comparison of morphologies of pure PMMA/PU IPNs synthesized during 10 min and 1 h

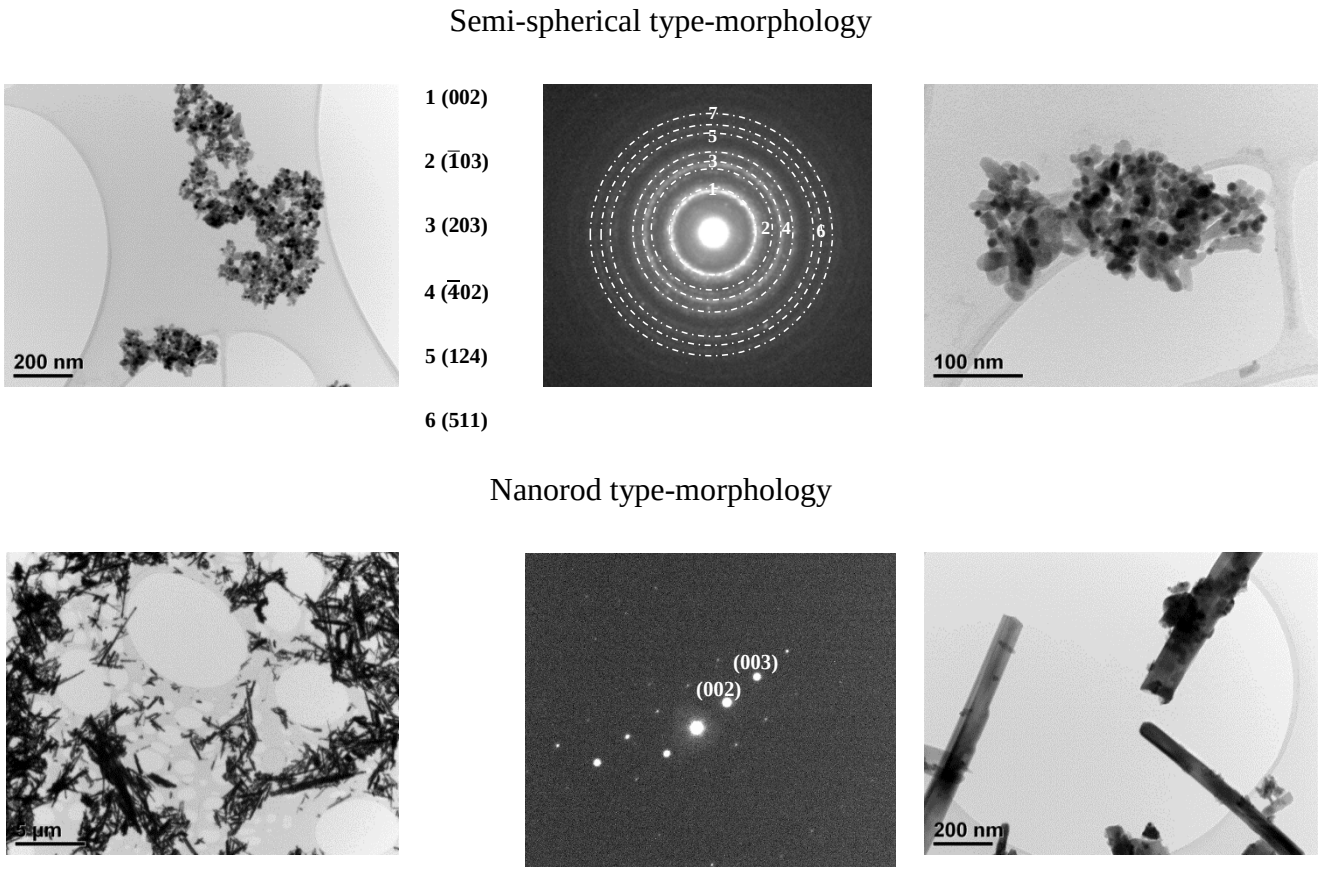

Figure 3. TEM micrographs and SAED patterns of $CePO_4$ in nanorods (pH 1) and semi-spherical (pH 11) morphologies

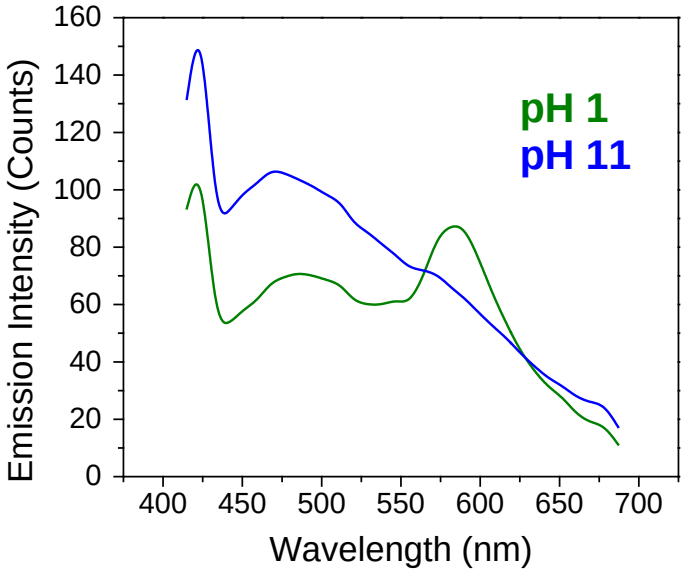

Figure 4. Fluorescence of $CePO_4$ in nanorods (pH 1) and semi-spherical (pH 11) type morphologies

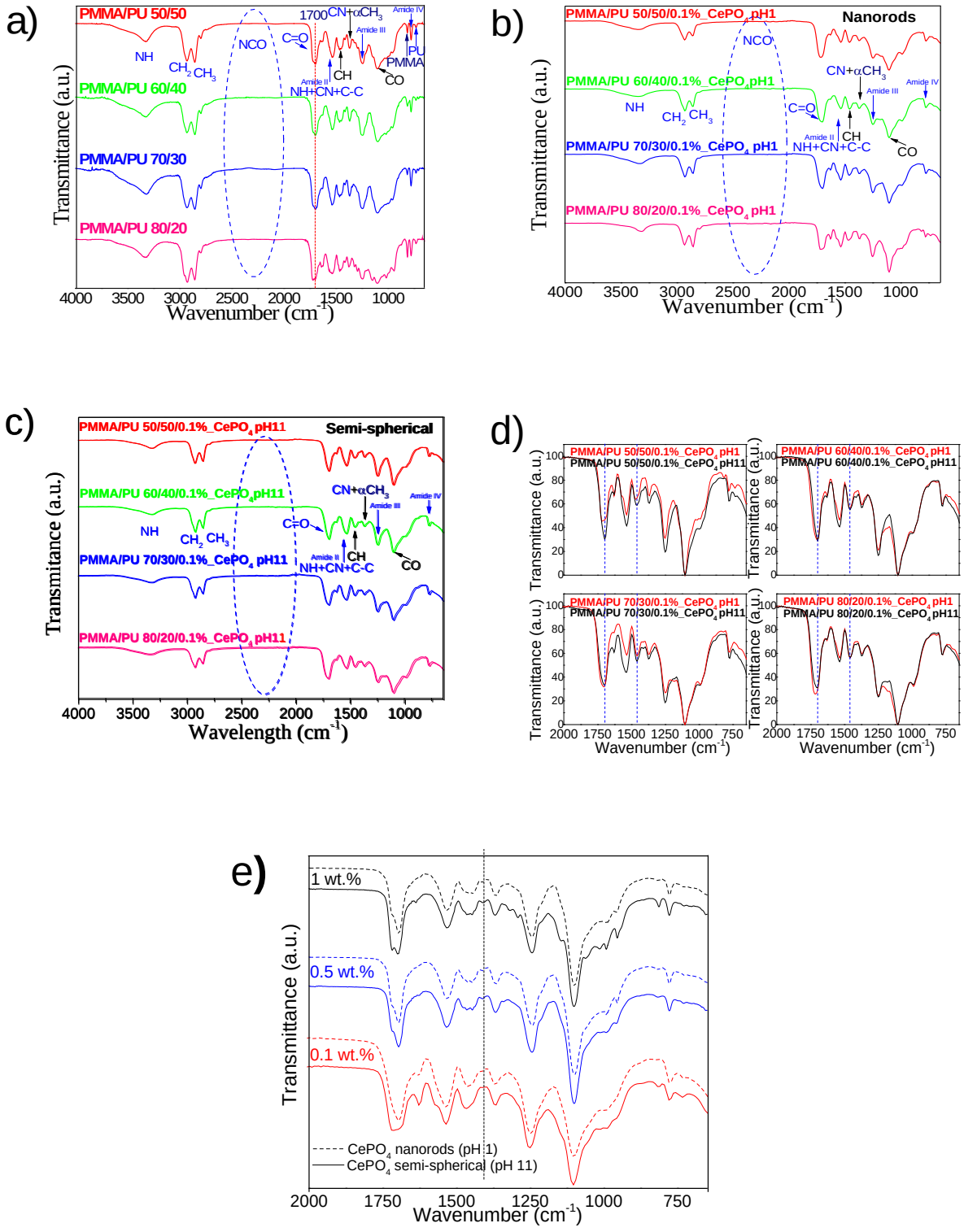

Figure 5. FT-IR spectra of a) PMMA/PU IPN b) PMMA/PU/$CePO_4$(pH 1) IPNs, c) PMMA/PU/$CePO_4$(pH 11) IPNs and d) Comparison between the addition of 0.1 wt.% $CePO_4$ pH 1 and pH 11, e) Comparison between the addition of 0.1, 0.5 and 1 wt.% in PMMA/PU 50/50.

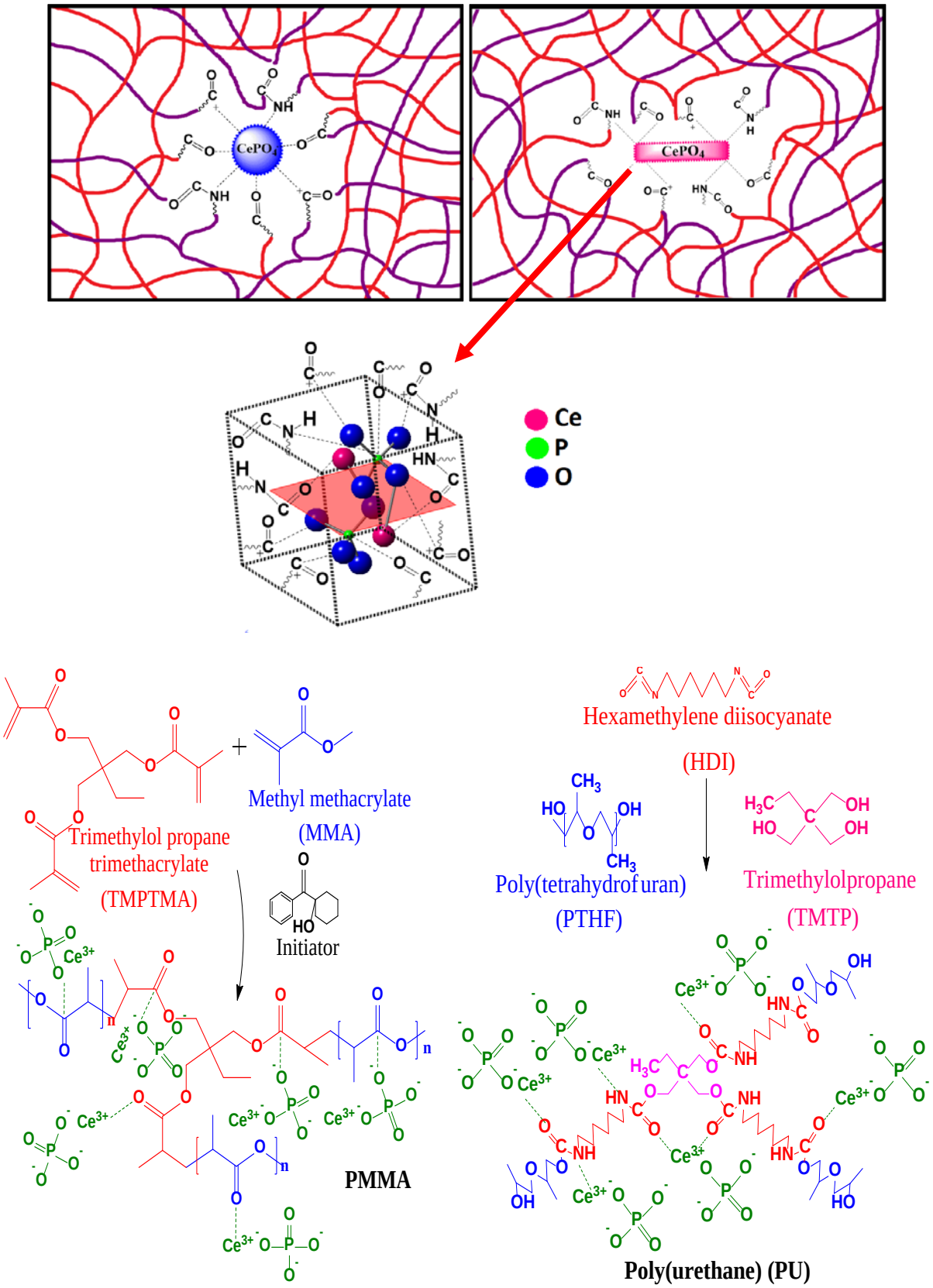

Figure 6. Representation of physical interaction between $CePO_4$ nanostructures and PMMA/PU IPN.

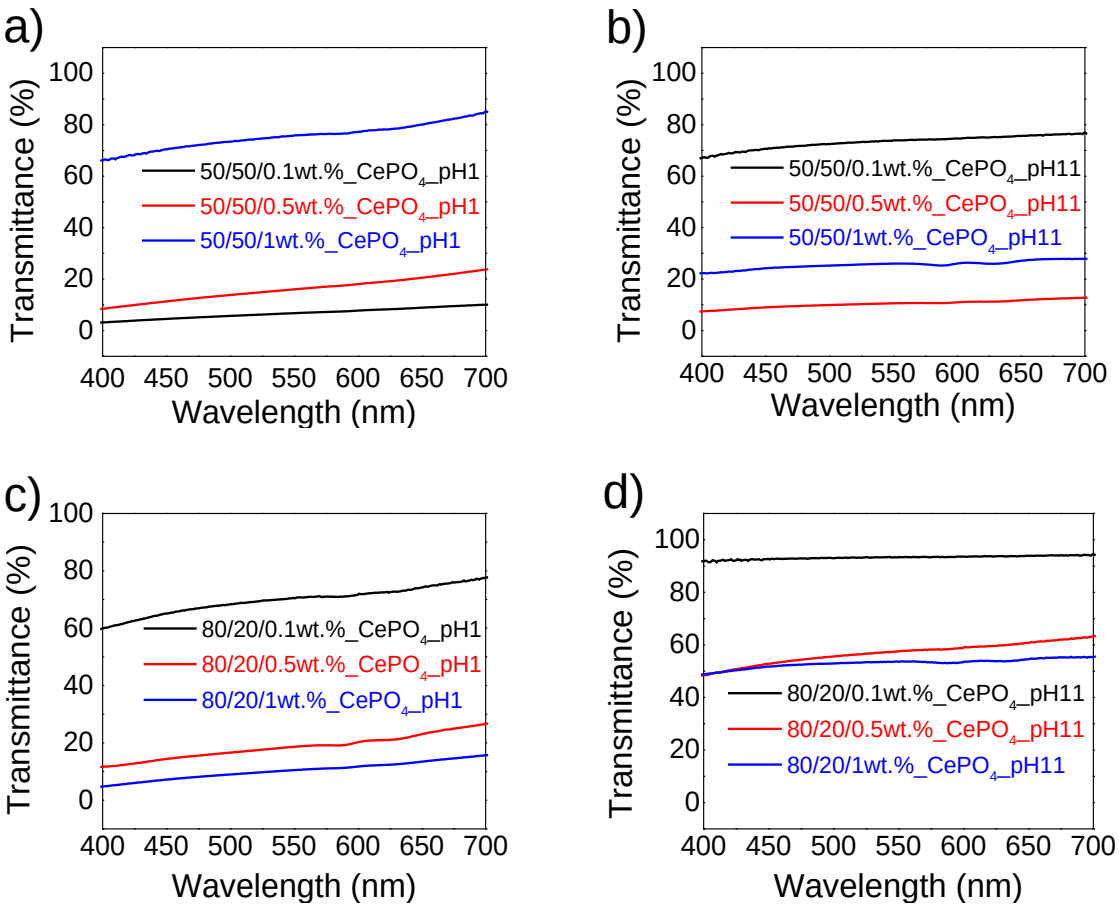

Figure 7. Visible spectra of PMMA/PU/$CePO_4$ IPNs

PMMA/PU (50/50)/$CePO_4$ Nanorods (0.1 wt.%)

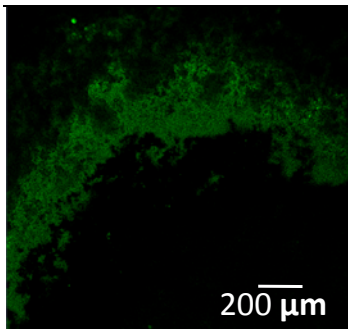

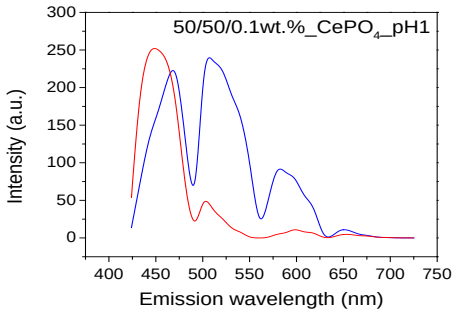

PMMA/PU (60/40)/$CePO_4$ Nanorods (0.1 wt.%)

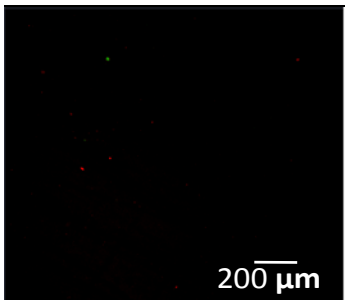

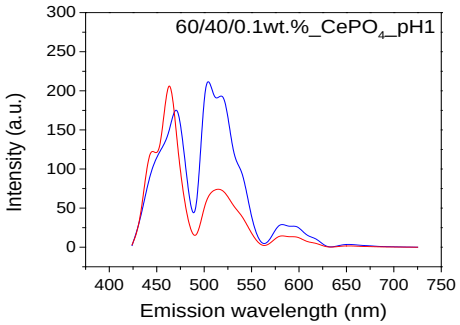

PMMA/PU (70/30)/$CePO_4$ Nanorods (0.1 wt.%)

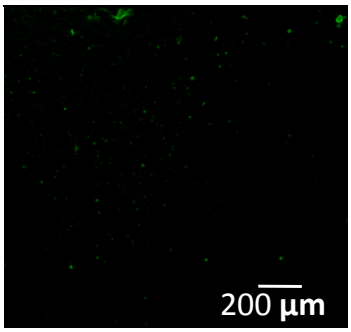

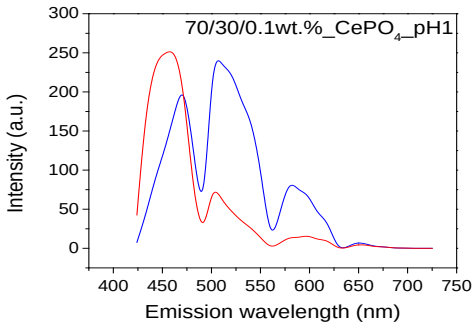

PMMA/PU (80/20)/$CePO_4$ Nanorods (0.1 wt.%)

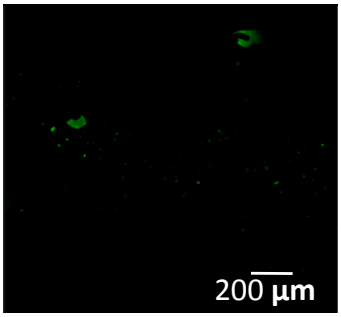

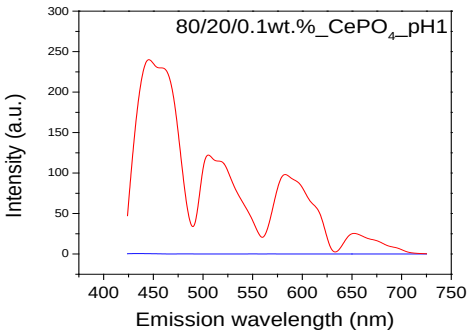

Figure 8. CLSM micrographs with their corresponding emission spectra of $CePO_4$ nanorods in 0.1 wt.% into 50/50, 60/40, 70/30 and 80/20 ratio of PMMA/PU IPNs.

PMMA/PU (60/40)/$CePO_4$ Semi-spherical (0.1 wt.%)

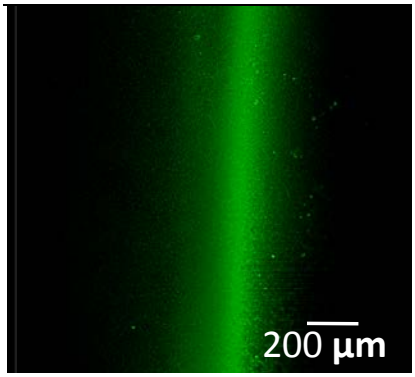

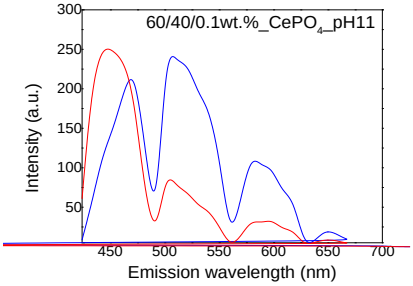

PMMA/PU (70/30)/$CePO_4$ Semi-spherical (0.1 wt.%)

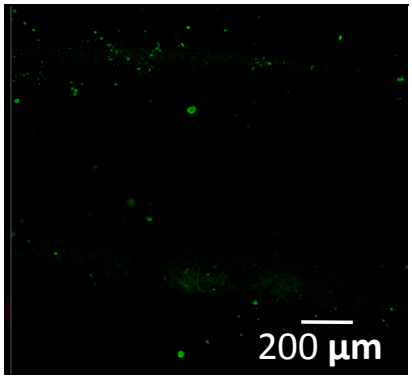

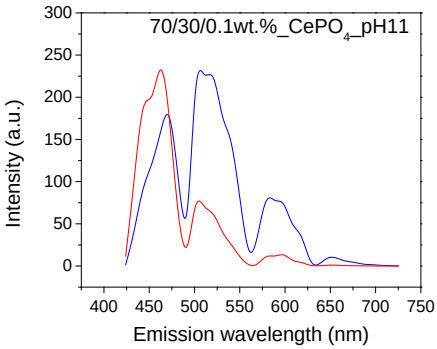

PMMA/PU (80/20)/$CePO_4$ Semi-spherical (0.1 wt.%)

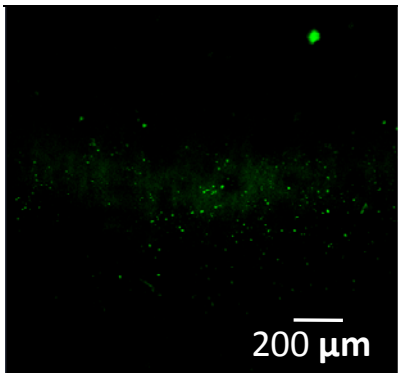

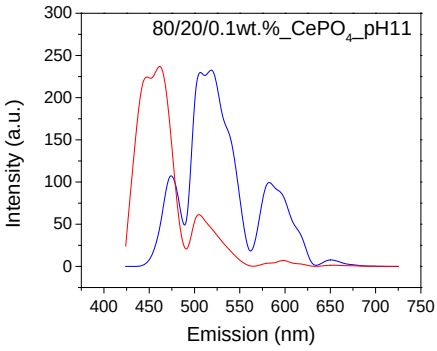

Figure 9. CLSM micrographs with their corresponding emission spectra of $CePO_4$ semi-spherical in 0.1 wt.% into 50/50, 60/40, 70/30 and 80/20 ratio of PMMA/PU IPNs.

PMMA/PU(50/50)/$CePO_4$ nanorods

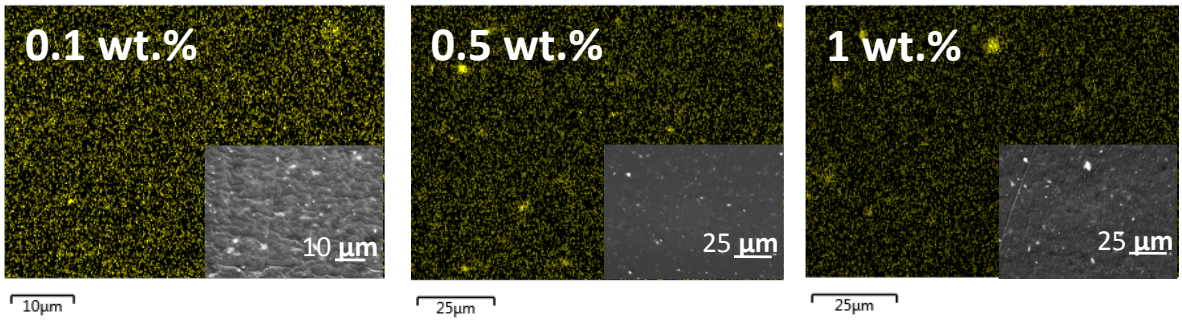

PMMA/PU(50/50)/$CePO_4$ Semi-spherical

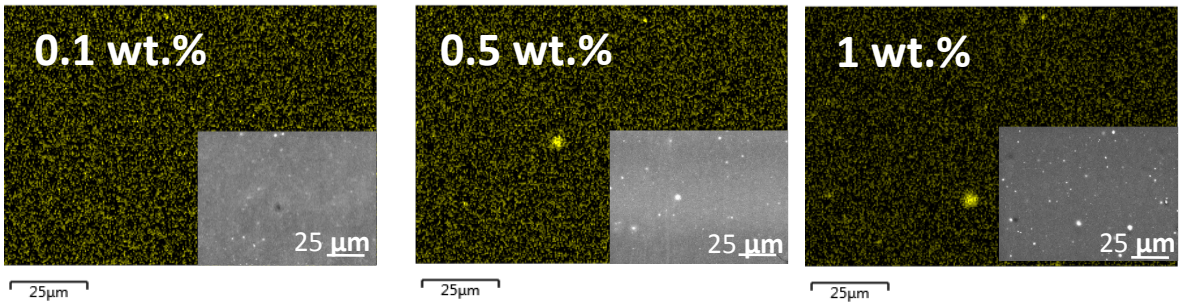

PMMA/PU(80/20)/$CePO_4$ nanorods

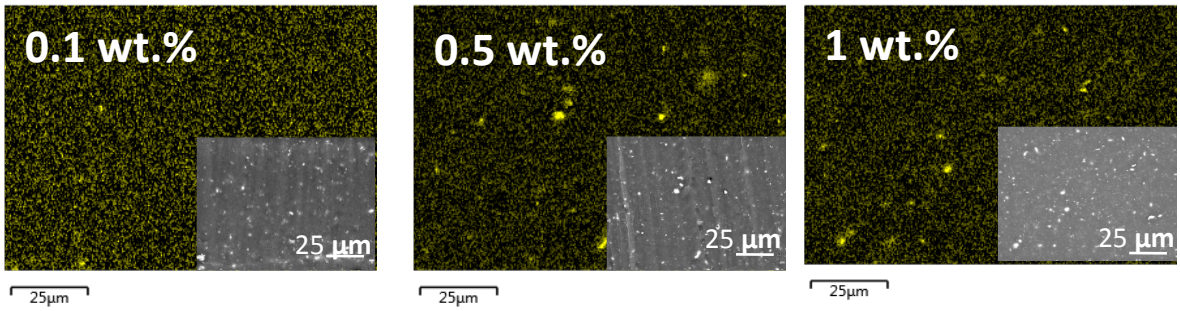

PMMA/PU(80/20)/$CePO_4$ Semi-spherical

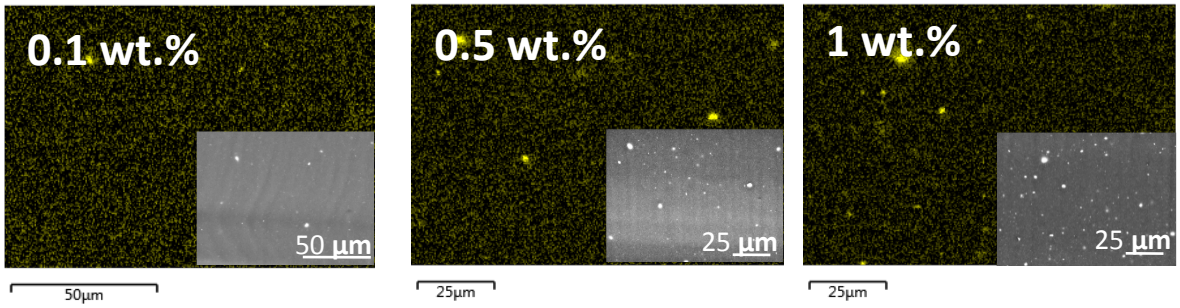

Figure 10. Representative SEM micrographs with their corresponding Cerium EDS elemental dot mapping of the addition of nanorods and semi-spherical nanoparticles in 0.1, 0.5 and 1 wt.% into 50/50 and 80/20 ratio of PMMA/PU IPNs.

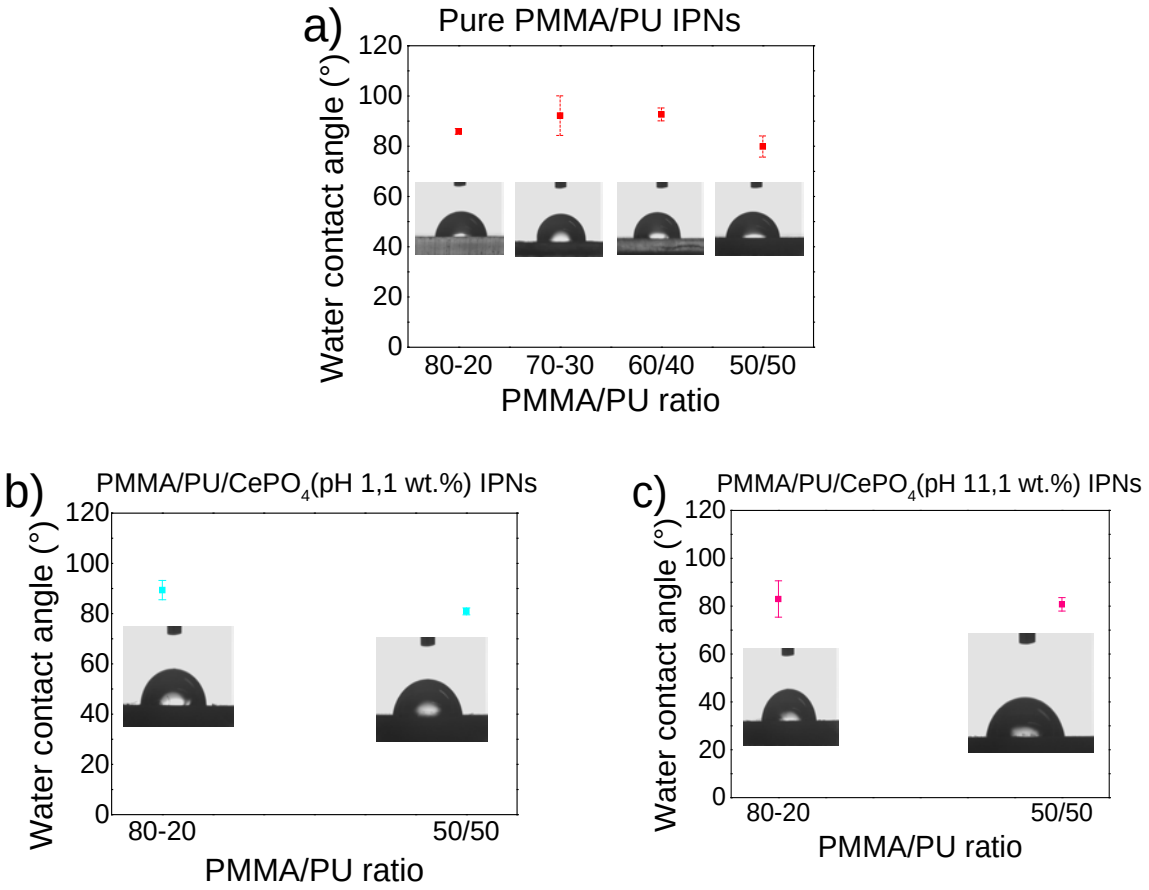

Figure 11. Water contact angle testing of selected PMMA/PU IPNs: a) pure PMMA/PU IPNs, b) PMMA/PU/$CePO_4$ (nanorods) IPNs and c) PMMA/PU/$CePO_4$ (semi-spherical)

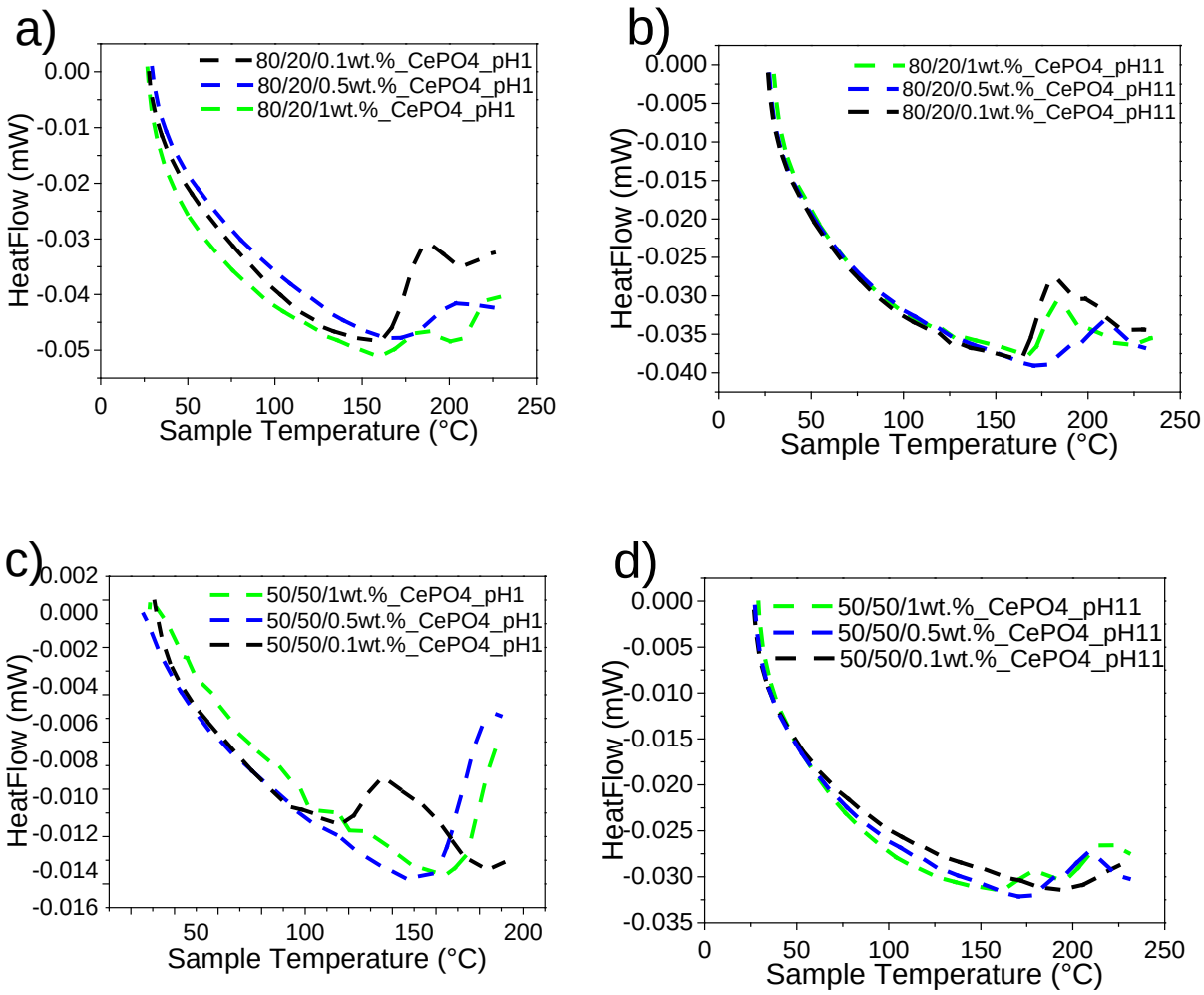

Figure 12. DSC thermograms of a) PMMA/PU(80/20)/nanorods_$CePO_4$, b) PMMA/PU(80/20)/semi-spherical_$CePO_4$, c) PMMA/PU(50/50)/nanorods_$CePO_4$ and d) PMMA/PU(50/50)/semi-spherical_$CePO_4$.

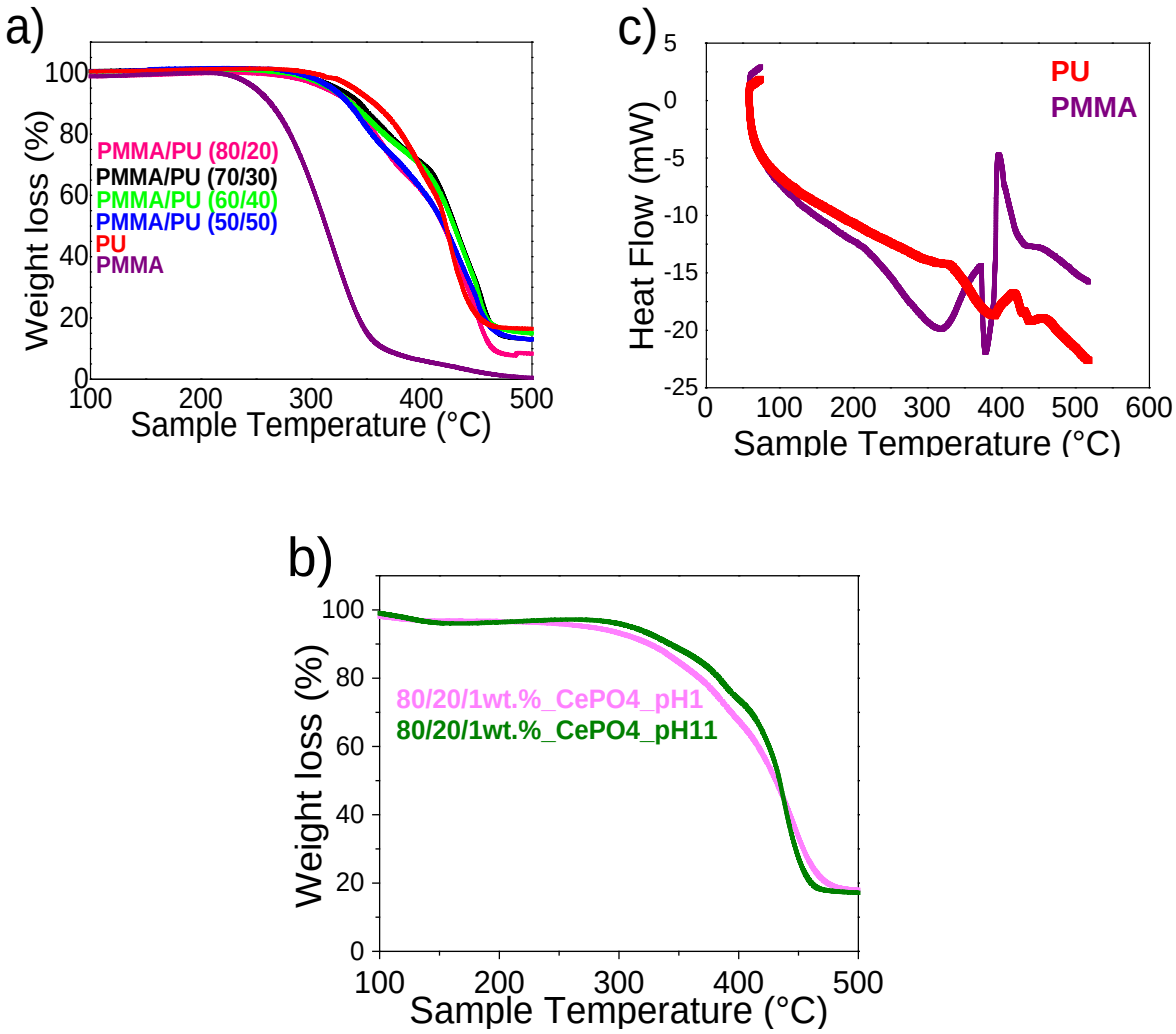

Figure 13. TGA thermograms of a) pure PMMA/PU IPNs, b) DTGA of PMMA and PU and c) TGA thermograms of comparison between PMMA/PU/$CePO_4$ with the addition of 1 wt.% of nanorods and semi-spherical

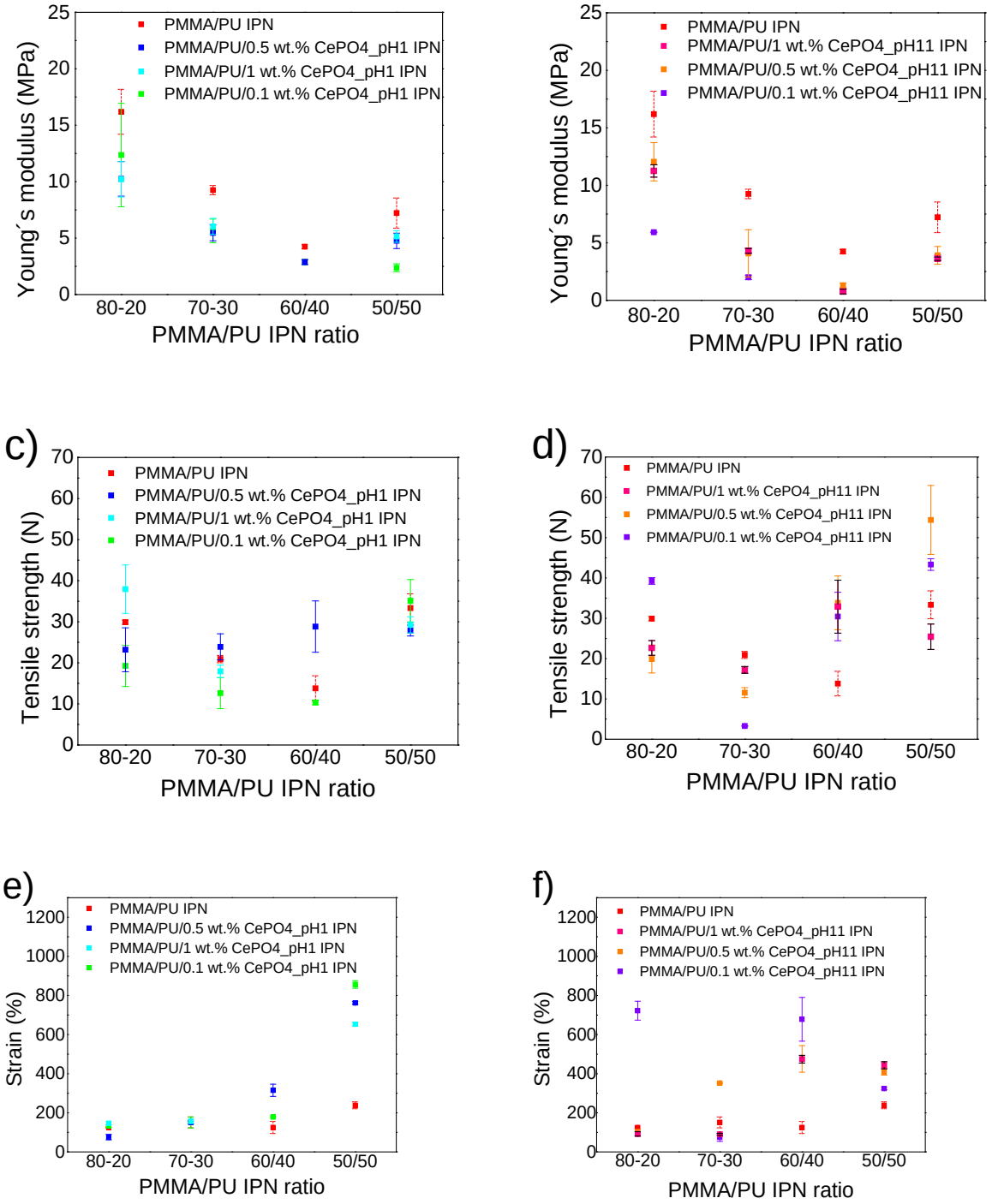

Figure 14. Mechanical properties pure PMMA/PU and PMMA/PU/$CePO_4$ IPNs

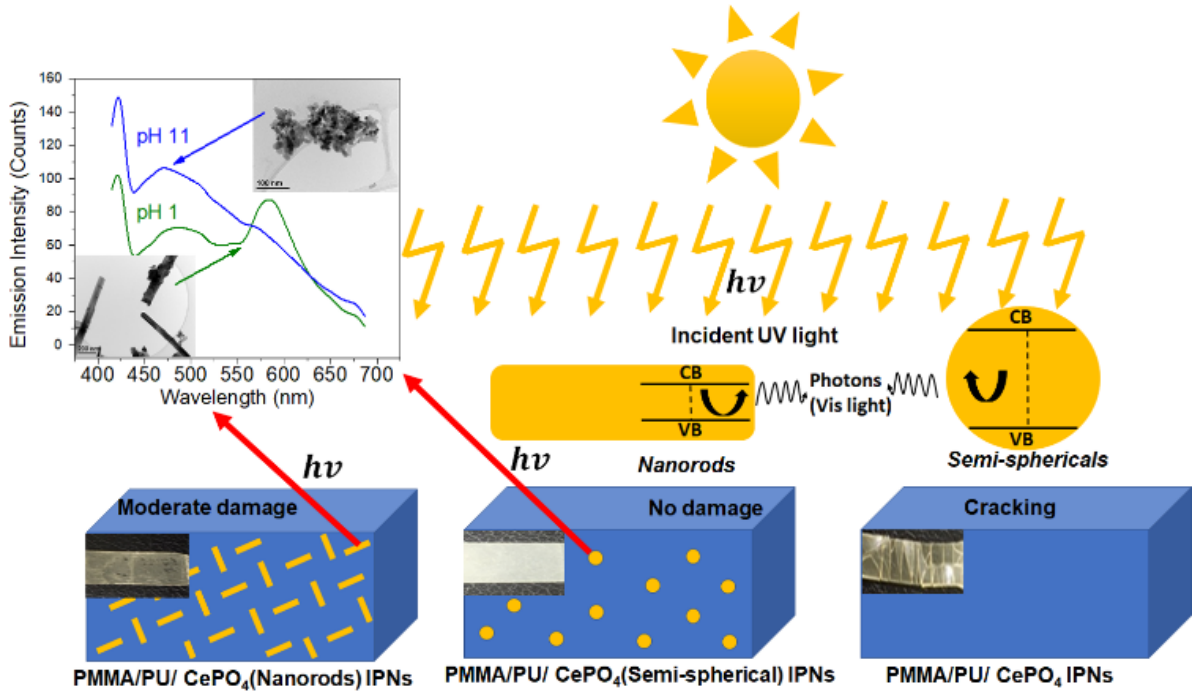

Figure 15. Luminescent mechanism of PMMA/PU/$CePO_4$ under UV light.

Tables.

Table 1. Data of thermal transitions detected in DSC thermograms of PMMA/PU and PMMA/PU/$CePO_4$.

PMMA/PU ratio	Addition of $CePO_4$ (wt.%)	Type of morphology		Tg (°C)	Area under peak 1 (mW)	Area under peak 2 (mW)	(Tp_1) (°C)	(Tp_2) (°C)	Interval peak 1 (°C)	Interval peak 2 (°C)
		Nanorods	Semi-spherical							
$50/50_{10min}$	---	---	---	130	---		---		---	
50/50	---	---	---	148	---	---	---	---	---	---
50/50	0.1	X		124	0.12378	---	160	---	131-212	---
50/50	0.5	X		123	0.15759	---	186	---	155-189	---
50/50	1	X		120	0.41217	---	182	---	154-222	---
50/50	0.1		X	123	---	---	---	---	---	---
50/50	0.5		X	124	0.00338	0.03348	187	209	179-196	198-227
50/50	1		X	123	0.01968	0.03961	176	215	161-192	198-230
$60/40_{10min}$	---	---	---	125	---	---	---	---	---	---
60/40	---	---	---	125	---	---	---	---	---	---
$70/30_{10min}$	---	---	---	---	---	---	---	---	---	---
70/30	---	---	---	126	---	---	---	---	---	---
$80/20_{10min}$	---	---	---	123	---	---	---	---	---	---
80/20	---	---	---	123	---	---	---	---	---	---
80/20	0.1	X		124	0.22685	---	185	---	160-210	---
80/20	0.5	X		124	0.10205	---	204	---	177-228	---
80/20	1	X		124	0.03809	0.01625	183	220	165-200	207-229
80/20	0.1		X	124	0.07426	0.00528	180	202	162-195	196-213
80/20	0.5		X	124	0.00363	0.03521	187	209	177-196	200-227
80/20	1		X	124	0.04835	0.0218	179	201	163-192	194-211

Table 2. Poly(urethane) **v**ibrational bands (in cm^{-1}) observed in FTIR spectra and their assignments.

Wavenumber (cm^{-1})	**Assignment**
3323	NH Stretching vibration
2934, 2853 and 2798	CH Stretching: antisymmetric stretching mode and symmetric stretching of methylene groups and O-CH_2 stretching
1700	Amide I: C=O stretching vibration
1532	Amide II, NH in-plane deformation + C-N and C-C stretching)
1464	CH_2 scissoring and CH_3 deformation
1367	C-N stretching
1248	Amide III: C-N stretching
1100	C-O-C stretching vibration of ether group
778	Amide IV

Table 3. Poly(methyl methacrylate) **v**ibrational bands (in cm^{-1}) observed in FTIR spectra and their assignments

Wavenumber (cm^{-1})	**Assignment**
3020-2850	C-H stretching of CH_3 and CH_2 groups
1716	Ester carbonyl group stretching
1450	C-H bending of CH_3 bonds
1210-1320	C-O-C stretching
1145	C-O-C stretching
1382 and 751	α-CH_3 bending
990	O-CH_3 Out-of-plane deformation
960-650	C-H Bending

Table 4. Mechanical properties of pure PMMA/PU and PMMA/PU/$CePO_4$ IPNs

PMMA/PU Ratio	of $CePO_4$ addition (wt.%)	Type of morphology		Young´s Modulus (MPa)	Tensile strength (N)	Deformation (%)
		Nanorods	Semi-spherical			
50/50	--	--	--	7.22 ± 1.33	33.34 ± 3.47	238.54 ± 17.77
50/50	0.1	X		2.37 ± 0.35	35.12 ± 5.16	856.16 ± 19.56
50/50	0.5	X		4.76 ± 0.68	30.19 ± 4.79	743.14 ± 6.76
50/50	1	X		5.15 ± 0.52	31.12 ± 4.49	658.34 ± 12.43
50/50	0.1		X	3.78 ± 0.16	43.33 ± 1.44	323.80 ± 5.63
50/50	0.5		X	3.91 ± 0.77	54.38 ± 8.56	409.48 ± 16.82
50/50	1		X	3.62 ± 0.15	30.91 ± 5.75	654.21 ± 36.37
60/40	--	--		4.24 ± 0.18	13.80 ± 3.05	142.64 ± 5.07
60/40	0.1	X		2.88 ± 0.22	9.46 ± 1.86	172.80 ± 5.98
60/40	0.5	X		2.45 ± 0.60	25.52 ± 8.35	315.16 ± 31.11
60/40	0.1		X	0.87 ± 0.14	32.08 ± 5.98	975 ± 57.92
60/40	0.5		X	1.30 ± 0.21	33.84 ± 6.69	760.94 ± 37.57
60/40	1		X	0.76 ± 0.20	33.96 ± 7.65	864.06 ± 2.21
70/30	--	--		9.25 ± 0.41	20.92 ± 0.88	67.95 ± 4.48
70/30	0.1	X		5.64 ± 1.05	14.26 ± 2.30	--149.68 ± 27.72
70/30	0.5	X		5.46 ± 0.70	23.89 ± 3.18	150.84 ± 6.67
70/30	1	X		6.04 ± 0.71	19.28 ± 2.33	156.00 ± 10.49
70/30	0.1		X	2.00 ± 0.19	3.26 ± 0.38	74.62 ± 20.51
70/30	0.5		X	4.08 ± 2.06	16.32 ± 8.28	452.76 ± 174.64
70/30	1		X	4.30 ± 0.21	17.19 ± 0.82	89.84 ± 4.79
80/20	--	--		16.19 ± 1.99	29.90 ± 0.50	124.84 ± 3.23
80/20	0.1	X		8.67 ± 1.57	27.80 ± 3.58	122.98 ± 20.47
80/20	0.5	X		10.25 ± 1.53	24.66 ± 5.42	78.16 ± 7.09
80/20	1	X		10.21 ± 1.57	35.47 ± 8.72	141.53 ± 33.05
80/20	0.1		X	6.90 ± 0.64	39.25 ± 0.83	722.14 ± 48.43
80/20	0.5		X	12.05 ± 1.67	22.79 ± 3.95	103.45 ± 9.10
80/20	1		X	11.25 ± 0.54	22.64 ± 1.78	91.98 ± 11.03

Table 5. Mechanical properties acquired from tensile test of pure PMMA/PU and PMMA/PU/$CePO_4$ IPNs after 500 h under accelerated aging test (heat and humidity conditions)

PMMA/PU ratio	wt.% of $CePO_4$ addition	Type of morphology		Young´s Modulus	Tensile strength	Elongation
		Nanorods	Semi-spherical	(MPa)	(N)	(%)
50/50				6.36 ± 0.65	13.50 ± 3.67	70.52 ± 12.42
50/50	0.1	X		5.776± 0.57	11.97 ± 1.83	56.67 ± 16.19
50/50	0.5	X		2.86 ± 0.31	8.05 ± 0.31	82.46 ± 18.19
50/50	0.1		X	3.81 ± 0.37	15.14 ± 2.11	156.93 ± 17.91
50/50	0.5		X	3.89 ± 0.46	7.64 ± 1.52	75.82 ± 19.65
80/20				10.68 ± 2.15	10.00 ± 1.51	37.42 ± 5.71
80/20	0.1	X		8.75 ± 0.59	12.49 ± 2.21	44.94 ± 9.09
80/20	0.5	X		8.24 ± 0.75	12.00 ± 3.91	37.93 ± 8.17
80/20	0.1		X	1.12 ± 0.15	29.85 ± 2.85	689.09 ± 38.73
80/20	1		X	14.57 ± 1.71	12.45 ± 2.52	29.33 ± 3.03

Table 6. Mechanical properties acquired from nanoindentation test of selected PMMA/PU/$CePO_4$ IPNs after 500 h under accelerated weathering test (UV light and humidity conditions)

PMMA/PU ratio	$CePO_4$ Wt. % of addition	Type of morphology		HIT (Mpa)	EIT (Gpa)
		Rods	Semi-spherical		
50/50	0.1		X	0.0195±0.0441	0.0083±0.0010
$50/50_{ACW}$	0.1		X	0.0431±0.0431	0.0085±0.0039
80/20	0.1	X		1.3699±0.2612	0.0081±0.0008
$80/20_{ACW}$	0.1	X		3.2363±0.4365	0.0347±0.0028
80/20	0.1		X	2.5837±0.4614	0.0164±0.0021
$80/20_{ACW}$	0.1		X	2.7624±0.4873	0.0153±0.0014